

# **Coastal Land Loss and Wave-Surge Predictions During Hurricanes in Coastal Louisiana: Implications for the Oil and Gas Industry**

## **Project Principal Investigators:**

**Dr. Gregory W. Stone<sup>1,2</sup>**  
**James P. Morgan Distinguished Professor**

**Dr. Alex Sheremet<sup>1,2</sup>**  
**Assistant Professor**

**Xiongping Zhang<sup>1</sup>**  
**Research Associate**

**DeWitt Braud<sup>3</sup>**  
**Research Associate**

## **With Assistance Provided by:**

**Gregory Steyer<sup>4</sup>**  
**John Barras<sup>4</sup>**  
**Dr. James B. Johnston<sup>4</sup>**  
**Susan Childs<sup>5</sup>**  
**Katherine Vaughan<sup>6</sup>**

<sup>1</sup>Coastal Studies Institute

<sup>2</sup>Department of Oceanography and Coastal Sciences

<sup>3</sup>Department of Geography and Anthropology

Louisiana State University

Baton Rouge, LA 70803

<sup>4</sup>United States Geological Survey, National Wetlands Research Center

<sup>5</sup>Minerals Management Service

<sup>6</sup>Louisiana Department of Natural Resources

**Final Project Report Prepared for:**  
**Louisiana Department of Natural Resources**  
**U.S. Geological Survey**  
**U.S. Minerals Management Service**  
**February 14, 2003**

# **Coastal Land Loss and Wave-Surge Predictions During Hurricanes in Coastal Louisiana: Implications for the Oil and Gas Industry**

## **Project Principal Investigators:**

**Dr. Gregory W. Stone<sup>1,2</sup>**  
**James P. Morgan Distinguished Professor**

**Dr. Alex Sheremet<sup>1,2</sup>**  
**Assistant Professor**

**Xiongping Zhang<sup>1</sup>**  
**Research Associate**

**DeWitt Braud<sup>3</sup>**  
**Research Associate**

## **With Assistance Provided by:**

**Gregory Steyer<sup>4</sup>**  
**John Barras<sup>4</sup>**  
**Dr. James B. Johnston<sup>4</sup>**  
**Susan Childs<sup>5</sup>**  
**Katherine Vaughan<sup>6</sup>**

<sup>1</sup>Coastal Studies Institute

<sup>2</sup>Department of Oceanography and Coastal Sciences

<sup>3</sup>Department of Geography and Anthropology

Louisiana State University

Baton Rouge, LA 70803

<sup>4</sup>United States Geological Survey, National Wetlands Research Center

<sup>5</sup>Minerals Management Service

<sup>6</sup>Louisiana Department of Natural Resources

**Final Project Report Prepared for:**  
**Louisiana Department of Natural Resources**  
**U.S. Geological Survey**  
**U.S. Minerals Management Service**  
**February 14, 2003**

## TABLE OF CONTENTS

<b>LIST OF FIGURES .....</b>	<b>II</b>
<b>LIST OF TABLES.....</b>	<b>IV</b>
<b>EXECUTIVE SUMMARY .....</b>	<b>V</b>
<b>INTRODUCTION.....</b>	<b>1</b>
Background.....	1
Objectives .....	2
Study Site Selection .....	2
Project Uniqueness.....	7
<b>METHODS AND NUMERICAL MODEL APPLICATION.....</b>	<b>12</b>
Introduction .....	12
Selection of an Historic Hurricane .....	12
Tropical Storm Wind Field Model .....	13
Numerical Model ADCIRC .....	16
Numerical Model SWAN.....	20
Input Data Preparation for ADCIRC.....	21
Input Data Preparation for SWAN .....	21
Output from ADCIRC .....	21
Output from SWAN .....	21
<b>RESULTS and DISCUSSION.....</b>	<b>23</b>
Surge Elevations and Wave Heights .....	23
Change in Surge and Wave Height: 1950 - early 1990's .....	30
Change in Surge and Wave Height: Early1990's – 2020 .....	36
Change in Surge and Wave Height: 1950 – 2020 .....	36
Degree of Surface Area Inundation.....	44
Geo-Spatial Analysis .....	46
Petroleum Product Storage Stations and Terminals from LDEQ EIS source data.....	46
Natural Gas Production and Distribution Facilities .....	46
Crude Petroleum and Natural Gas Production and Extraction Operations from LDEQ EIS source data..	48
Oil and Gas Well Locations, Current Record Version 04/07/1999, Louisiana Department of Natural Resources, Office of Conservation.....	48
Oil and Gas Platform Structures in the Gulf of Mexico from MMS source data.....	48
Oil and Gas Structures .....	50
Pipelines .....	50
Composites and Other Layers .....	50
<b>SUMMARY and CONCLUSIONS .....</b>	<b>57</b>
<b>REFERENCES .....</b>	<b>59</b>

## LIST OF FIGURES

Figure 1. Upper: An example of the frequency of landfalls of hurricanes in the Atlantic basin over a one hundred year period. Lower: Example of the spatial distribution of hurricane trajectories and landfalls for the same time period in the Gulf of Mexico.....	3
Figure 2. Tropical storm and hurricane strikes from Texas to Florida for the period 1900-2000 (From Muller and Stone, 2001). .....	4
Figure 3. Upper: Raccoon Island along the Isles Dernieres located in South-central Louisiana in 1992 before landfall of Hurricane Andrew. Lower: The same island after landfall of Andrew showing complete removal of sand from the barrier. ....	5
Figure 4. Left: Oblique aerial of breaching along the Isles Dernieres (Louisiana) after Hurricane Andrew. Right: Aerial of a Florida Panhandle barrier after impacts of Hurricane Opal. Both hurricanes were category 3 in strength at landfall (after Stone et al., 1995a; 1995b). .....	6
Figure 5. Numerically derived wave field under fairweather, deep water wave conditions along the Isles Dernieres. Note increase in wave height behind the barriers with time as the barrier system erodes. The simulated restored barriers demonstrate the importance of barriers in reducing wave energy in these bays and, therefore, marsh protection.....	8
Figure 6. Numerically derived wave field under fairweather, deep water wave conditions along the Isles Dernieres. Note increase in wave height behind the barriers with time as the barrier system erodes. The simulated restored barriers demonstrate the importance of barriers in reducing wave energy in these bays and, therefore, marsh protection.....	9
Figure 7. Location of study site in south-central Louisiana including Isles Dernieres and Timbalier islands, north to Lake Pelto. Note, this section of the coast is eroding at the highest rates in Louisiana and the nation. The red sequence of arrows shows the path of the hurricane modeled in this study.....	10
Figure 8. Left: Coastal configuration in 1950 where the study site had ~1.09 million acres of land. Middle: Study site in the early 1990's where the study site had been reduced to ~0.85 million acres of land, a 24% reduction. Right: Forecast loss of land in the study site by the year 2020. ....	11
Figure 9. Trajectory of the 1915 storm used in this study after the track is perturbed 0.9 degrees west in order to maximize the wind, surge and wave field at the study site. ....	14
Figure 10. Unstructured grid showing 49156 elements and 25108 nodes where bathymetry and topographic elevation values were obtained for modeling. ....	17
Figure 11. Map of spatially distributed data points for the Louisiana coast where depth and topographic values were obtained for modeling.....	18
Figure 12. Coarse (4 km, 2.5 mi) Gulf of Mexico basin scale and Fine (300 m, 985 ft) local scale encompassing the study site.....	19
Figure 13. Maximum storm surge elevation along the study site for the 1950 scenario.....	24
Figure 14. Maximum significant wave height distribution across the study site for the 1950 scenario.....	25
Figure 15. Distribution of maximum surge elevation and significant wave height across the study site for the 1950 sceanrio.....	26
Figure 16. Maximum storm surge elevation across the study site for the 1990's scenario.....	27
Figure 17. Maximum significant wave height distribution across the study site for the 1990's scenario.....	28
Figure 18. Maximum storm surge elevation and significant wave height distribution across the study site for the 1990's scenario.....	29
Figure 19. Maximum surge elevation across the study site for the 2020 scenario.....	31
Figure 20. Maximu m Significant Wave Height distribution across the study site for the 2020 scenario.....	32
Figure 21. Maximum Storm Surge Elevation and Significant Wave Height for the study area in the 2020 scenario.....	33
Figure 22. Change in Maximum Surge levels between 1950-1990's across the study area.....	34
Figure 23. Change in Significant Wave Height between 1950 and 1990's across the study area.....	35
Figure 24. Difference in Maximum Storm Surge and Significant Wave Height between 1950 and 1990's scenarios.....	37
Figure 25. Difference in Maximum Storm Surge between 1990's and 2020 scenarios.....	38
Figure 26. Difference in Maximum Significant Wave Height between 1990's and 2020 scenarios.....	39
Figure 27. Difference in Maximum Storm Surge and Maximum Wave Height between 1990's and 2020 scenarios.....	40

Figure 28. Difference in Maximum Storm Surge between 1950 and 2020 scenarios.....	41
Figure 29. Difference in Maximum Significant Wave Height between 1950 and 2020 scenarios. ....	42
Figure 30. Difference in Maximum Storm Surge and Maximum Wave Height between 1950 and 2020 scenarios.....	43
Figure 31. Surface area change of maximum surge (A), maximum significant wave height (B) and the composite of surge and wave height (C). Rate of surface area change of maximum surge (D), maximum significant wave height (E) and the composite of surge and wave height (F). ....	45
Figure 32. Distribution of crude petroleum and gas production facilities superimposed on the 1990's Maximum Storm Surge Elevation and Maximum Significant Wave Height composite.....	49
Figure 33. Distribution of oil and gas wells superimposed on the 1990's Maximum Storm Surge Elevation and Maximum Significant Wave Height composite.....	52
Figure 34. Distribution of platforms and structures superimposed on the 1990's Maximum Storm Surge Elevation and Maximum Significant Wave Height composite.....	53
Figure 35. Distribution of pipelines superimposed on the 1990's Maximum Storm Surge Elevation and Maximum Significant Wave Height composite. ....	54
Figure 36. Distribution of crude petroleum and gas production facilities superimposed on the 1990's Maximum Storm Surge Elevation and Maximum Significant Wave Height composite.....	55
Figure 37. Distribution of wells, pipelines, structures, platforms and facilities superimposed on the change in combined storm surge levels and wave heights for the period 1950-1990's. The green shades indicate an increase in surge and wave height combined. Note that for clarity those increases above 6 ft are not provided. The reader is referred to Figure 24 for a more detailed representation of change.	56

## LIST OF TABLES

Table 1. Oil and gas resources at risk, 1990 maximum surge plus wave height.....	47
Table 2. Oil and gas resources at risk, 1950-2020 maximum surge plus wave height difference.....	47

## EXECUTIVE SUMMARY

The potential negative impact of hurricane-generated storm surge and wave energy on the oil and gas infrastructure located in coastal Louisiana is enormous. This can be attributed to: (1) the extent and number of facilities located there; and (2) the fact that barrier islands and marshes have drastically diminished during recent history and are predicted to continue doing so in the absence of implementing well designed, large-scale restoration plans. It is the primary objective of this pilot study to evaluate, using state-of-the-art numerical hydrodynamics models, how the loss of barrier islands and wetlands affects storm surge and wave energy along a portion of the south-central Louisiana coast.

Using a Hurricane Planetary Boundary model, a storm surge model (ADCIRC) and wave model (SWAN), the resultant data indicate that the vast majority of the study site underwent a considerable increase in combined surge and wave height during the interval 1950-1990's on simulating a category 3 hurricane. This is an important period in time in that it represents the actual physical breakdown of the coast and to which the increase in surge and wave height can be directly attributed. Thus, the conclusion is important in that the data provide a highly unique data set demonstrating that the deterioration of coastal south-central Louisiana has likely resulted in an increase in surge and wave height during this 40-year time period. The magnitude of increase is typically 8-10 ft although change >12 ft is readily apparent along the marsh shorelines and barriers.

Over the approximate 30 year period between 1990's and 2020, the model forecast results also indicate that a significant increase in surge and wave height will occur throughout much of the study site. Increases are widespread in the study area with the largest occurring at Fourchon, Timbalier islands and in particular, Isles Dernieres and the adjacent marshes. At these locations increasing values range from 10 to >12 ft. Throughout the marsh north of Terrebonne Bay, values increase from 6 ft, although in several location increases between 10 and >12 ft were computed.

The data presented here have very important implications for the oil and gas infrastructure located in the study site. The data suggest that in the absence of large-scale barrier and marsh restoration, the current infrastructure will experience increasing surge levels and increasing wave energy if the anticipated coastal erosion is permitted to occur. The data dramatically illustrate that nearly the entire infrastructure is potentially exposed to increased surge and wave heights over time. It also important to note that this conclusion pertains to tropical storms and weaker hurricanes that historically, are known to have a high frequency of landfall along the Louisiana coast.

# INTRODUCTION

## Background

The south-central Louisiana coast is experiencing rapid deterioration of its barrier islands and mainland coast. Historically (past 100+ years), this coastal reach has undergone erosion along its Gulf-facing beaches at rates in excess of 50 ft. per year (McBride et al., 1992). Numerous scientific papers have concluded that Louisiana is experiencing the highest rates of coastal erosion in the United States (Gosselink et al., 1998). The forcing mechanisms responsible for such losses have been well documented and include rapid rise in relative sea-level, reduction in sediment supply to the coast, a host of complex physical processes and anthropogenic activity. A comprehensive review of the relative importance of these processes and human activities may be found in (Coleman et al., 1998).

Historical records suggest that the southeast of the U.S. experiences among the greatest number of tropical cyclone landfalls around the globe with the Gulf of Mexico experiencing a large number of them (Figure 1). In a recent study that focused on the frequency of tropical systems impacting the Louisiana coast, evidence was presented showing that along with Key West, Florida, south-central Louisiana ranked the highest over a one hundred year period (1900-2000) in frequency of strikes of major storms (category 3 and above) for an area extending from Texas to North Carolina (Muller and Stone, 2001). The distribution of strikes is shown for the Gulf of Mexico in Figure 2. Several recent scientific studies have underscored the significance of tropical and extratropical storms in driving coastal erosion along the Louisiana coast (Stone and Finkl, 1995; Stone et. al., 1993; 1995; 1997; 1999; 2003; Muller and Stone, 2001). As shown in Figure 3, winter storms in addition to tropical cyclones have frequently impacted the coast and more often than not, result in severe overwashing and breaching of the barrier and mainland systems. This is largely due to the fact that the elevation of the beach and dune system is exceptionally low, typically less than 10 ft. above sea level. Thus, the cumulative impact of these events over time is a gradual but significant decline in the physical stability of this coast. The combination of storms, sea level rise, subsidence and a reduction in sediment supply to the coast has resulted in rapid deterioration of the barrier islands in Louisiana. The islands are particularly vulnerable to breaching during storms and post-storm recovery is generally not accomplished, or slow between storm events. Figure 4 provides a contrast in response of a barrier in the Louisiana Isles Dernieres chain to Hurricane Andrew (1992) and a Florida Panhandle barrier's response to Hurricane Opal (1995). Note the breaching that occurred along the Louisiana barrier whereas the Florida barrier maintains its structural integrity. Both storms were comparable in strength and made landfall as category 3 hurricanes.

Reviews of the importance of hurricanes and tropical storms on coastal Louisiana can be found in (Penland et al, 1989; Stone et al, 1993; 1996; 1997; 1999; 2003). Recent work also shows that with the gradual demise of barrier islands along south-central Louisiana, wave energy conditions in the bays are increasing with time (Stone and McBride, 1998). This phenomenon is apparent during fair-weather wave conditions and

during storms when lower frequency waves propagate through wider inlets and breaches along the barrier system. A numerical wave modeling study (Stone and McBride, 1998) shows a positive correlation between barrier loss and bay wave energy increase very clearly. Forecasts of barrier island loss (Isles Dernieres and Timbalier island) between the 1990's through 2020 show dramatic increases in bay wave energy with time on simulating fairweather wave conditions (Figures 5 and 6). The importance of barrier restoration is also evident where a hypothetical barrier system is included in the numerical approach, and a dramatic decrease in wave energy in the bays occur. These data support the contention that if the outer coast is not restored, presently protected bay systems will be rapidly transformed into open marine conditions. Thus, marsh shorelines fringing these bays will continue to experience higher wave energy conditions over time, and thereby become increasingly prone to damage during severe storms including tropical storms and hurricanes.

## **Objectives**

While the connection between barrier loss and increased wave energy conditions during major storms in semi protected bays is intuitive, a detailed evaluation of this connection had not been made until now. Thus, the obvious implications for the oil and gas industry and increased vulnerability to waves and surge during major storms were not readily apparent. In late 2001 the Secretary of the Louisiana Department of Natural Resources commissioned a group of scientists at Louisiana State University to further evaluate this possibility. This report documents the methodological techniques and results of a study that focuses on the direct effects of barrier island and marsh loss on storm surge and wave energy levels associated with a major hurricane event. This effort was accomplished using state-of-the-art numerical wave and surge models. The project is viewed as a pilot effort that could be conducted over larger portions of the coast in the future.

## **Study Site Selection**

For purposes of this pilot project, the area shown in Figure 7 was chosen as the study site for several reasons: First, the site is characterized by a dense network of oil and gas infrastructure in the form of oil and gas wells, pipelines, platforms and structures, crude oil and gas production facilities. Second, Terrebonne Bay, in which much of this infrastructure exists, is fronted by the Isles Dernieres and Timbalier Island chains, both of which are eroding at among the highest rates in the State. As shown in Figures 5 and 6, this area is gradually being transformed into open marine conditions and the outer protective barrier system is becoming less efficient as a buffer to storm wave energy with time. As shown in Figure 8, the study site approximated 1.09 million acres in 1950. In the early 1990's, the area was reduced to approximately 0.85 million acres, a reduction of 24%. The panel on far right in Figure 8 shows the approximate landmass in accord with a forecast for the year 2020. While the 1950 and early 1990's surface is based on historical data sets, and therefore, the 24% reduction in landmass is real, the forecast to 2020 is simply an approximation. A more detailed evaluation of the techniques used to obtain this forecast can be obtained from Stone and McBride (1998) and the Barrier Island Feasibility Study (1999).

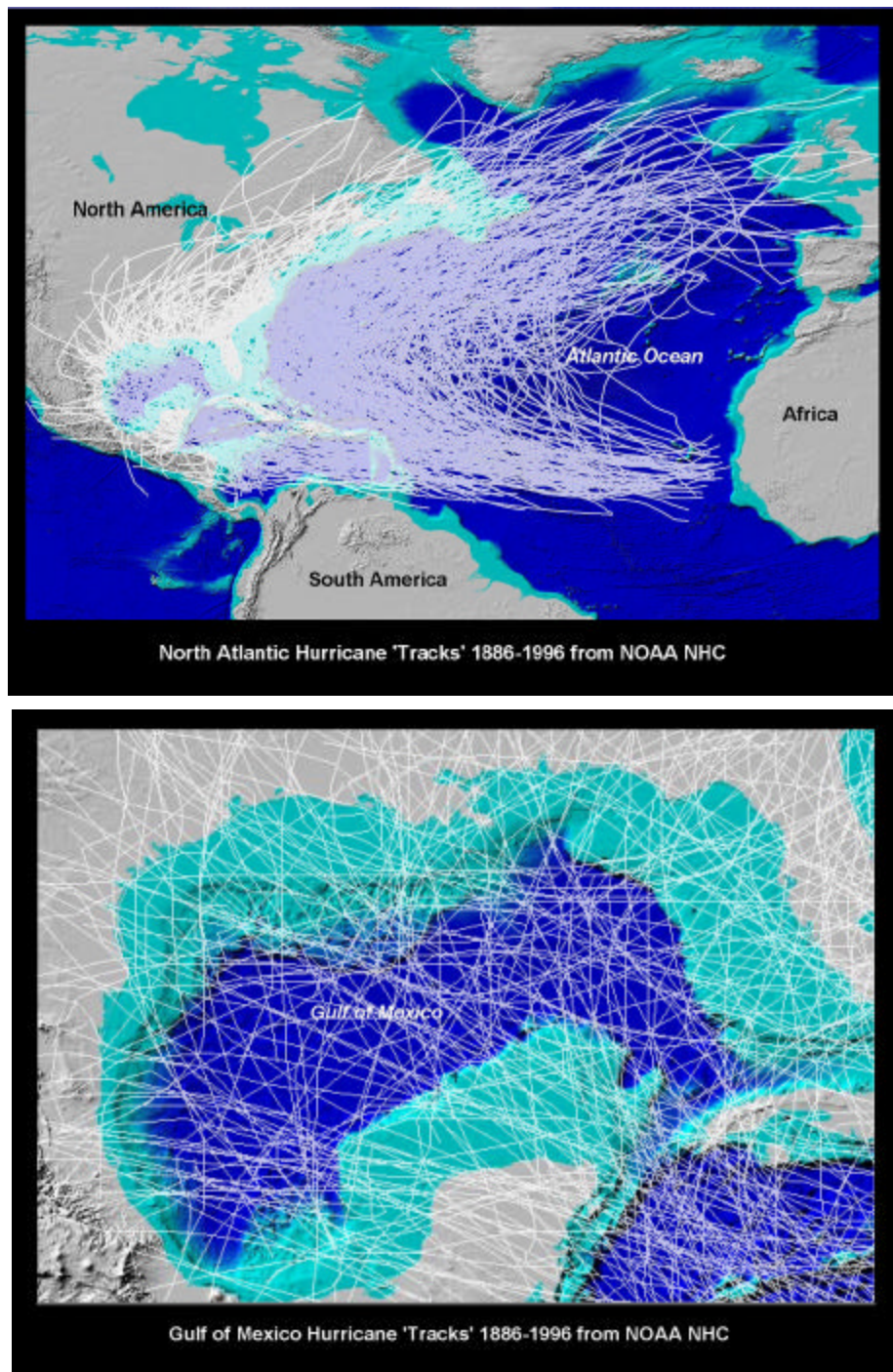


Figure 1. Upper: An example of the frequency of landfalls of hurricanes in the Atlantic basin over a one hundred year period. Lower: Example of the spatial distribution of hurricane trajectories and landfalls for the same time period in the Gulf of Mexico.

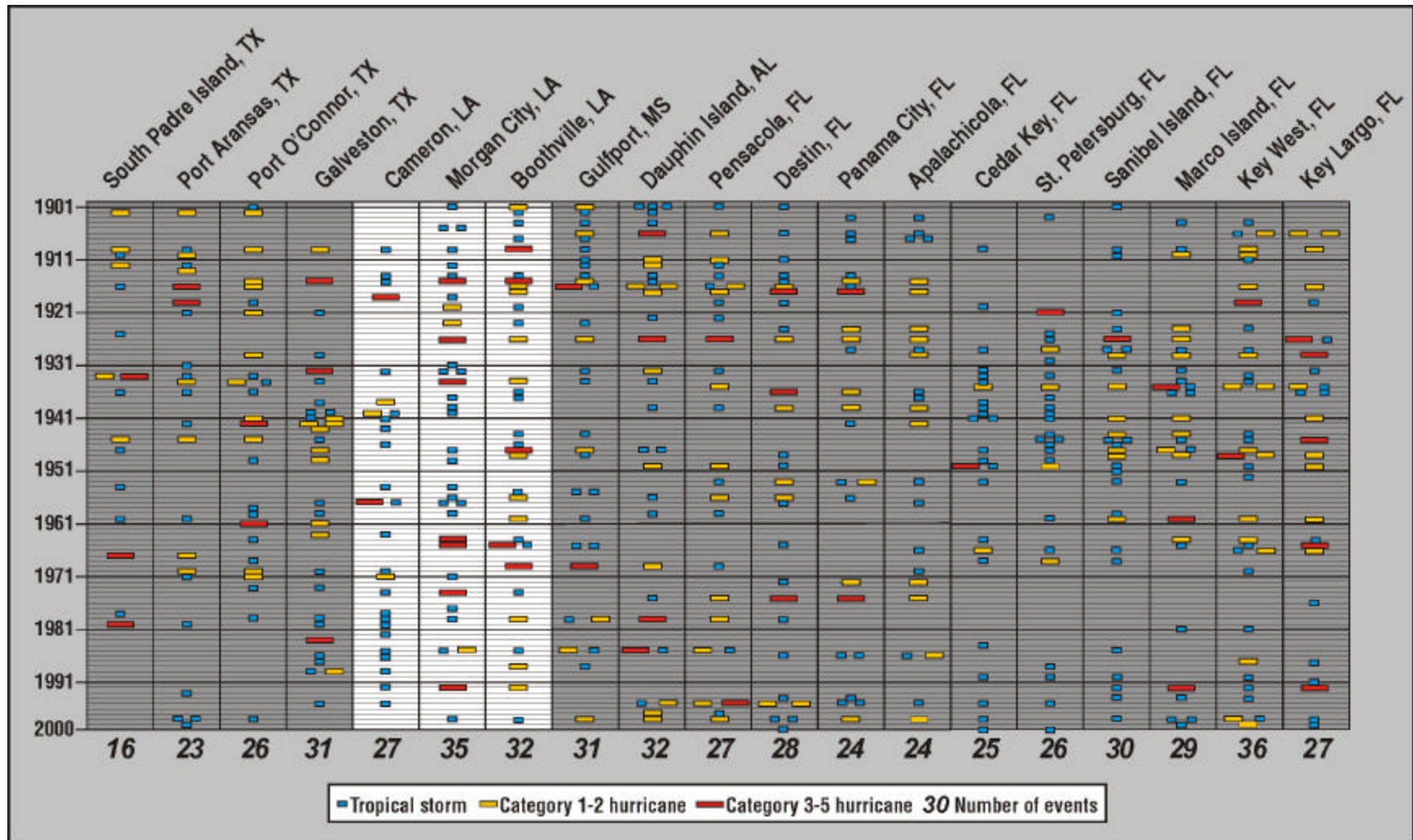


Figure 2. Tropical storm and hurricane strikes from Texas to Florida for the period 1900-2000 (From Muller and Stone, 2001).



Figure 3. Upper: Raccoon Island along the Isles Dernieres located in South-central Louisiana in 1992 before landfall of Hurricane Andrew. Lower: The same island after landfall of Andrew showing complete removal of sand from the barrier.



Figure 4. Left: Oblique aerial of breaching along the Isles Dernieres (Louisiana) after Hurricane Andrew. Right: Aerial of a Florida Panhandle barrier after impacts of Hurricane Opal. Both hurricanes were category 3 in strength at landfall (after Stone et al., 1995a; 1995b).

## **Project Uniqueness**

There are several reasons why this pilot project is deemed unique: (1) this is the first effort of its kind in Louisiana and in the nation that will quantitatively determine the connection between barrier island and wetland loss on the magnitude of change in storm surge and storm wave elevation; (2) the modeling approach utilizes state-of-the-science-numerical models (ADCIRC and SWAN) and goes beyond conventional approaches undertaken nationally to merely simulate storm surge, but includes storm waves also. Omitting wave propagation and wave height during such simulations significantly underestimates the resultant super-elevated water level during severe hurricanes; and (3) the project is a robust way by which the implications associated with changes in waves and storm surge over time can be evaluated with respect to the oil and gas industry.

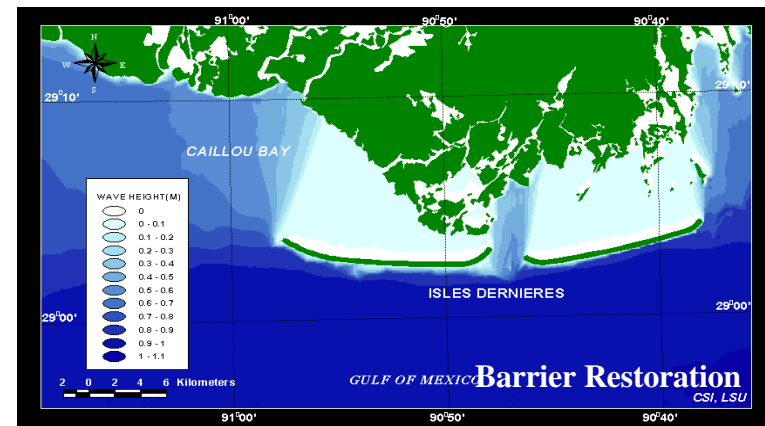
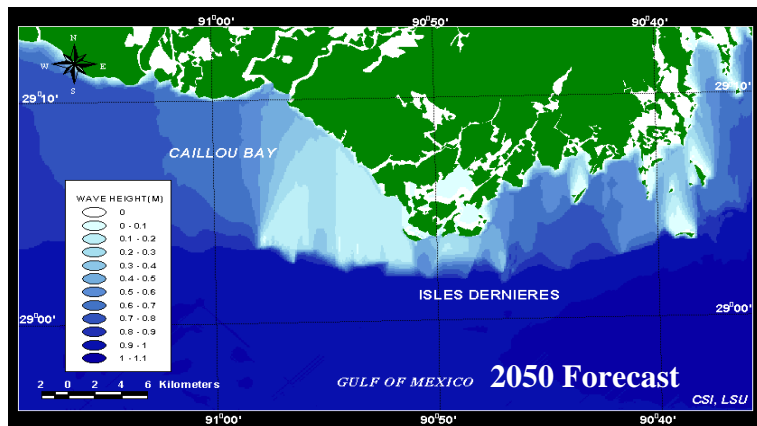
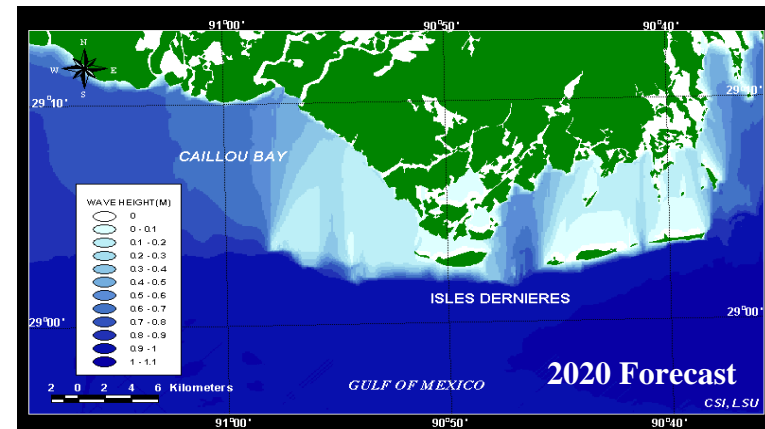
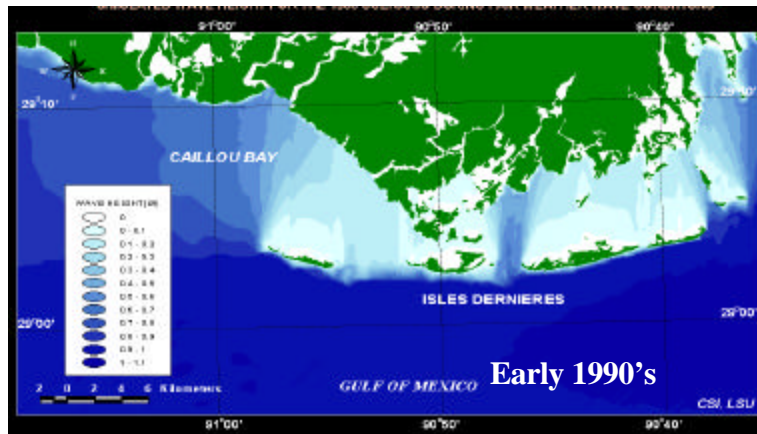


Figure 5. Numerically derived wave field under fairweather, deep water wave conditions along the Isles Dernieres. Note increase in wave height behind the barriers with time as the barrier system erodes. The simulated restored barriers demonstrate the importance of barriers in reducing wave energy in these bays and, therefore, marsh protection.

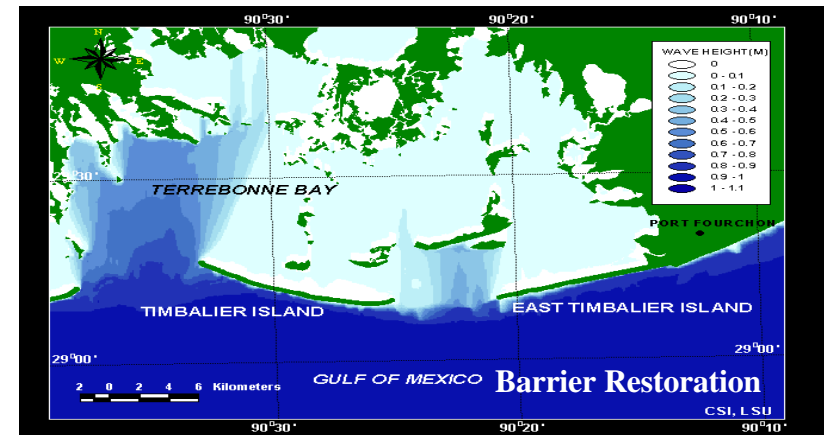
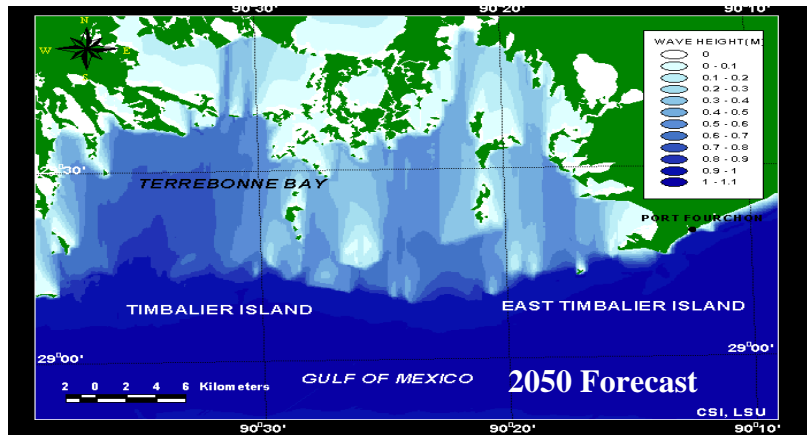
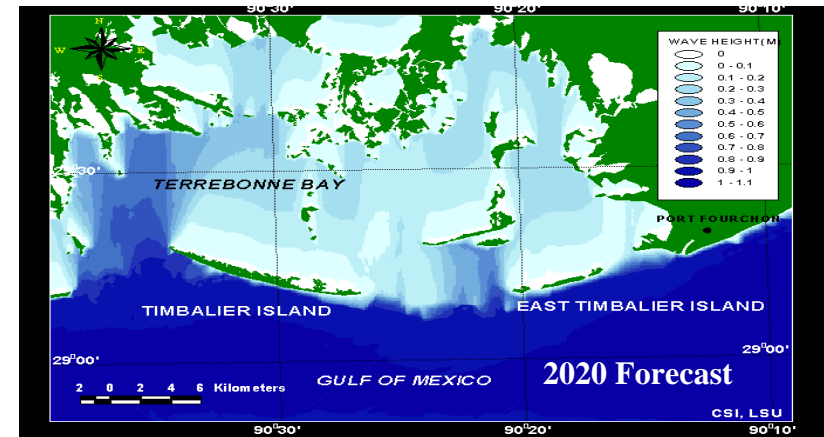
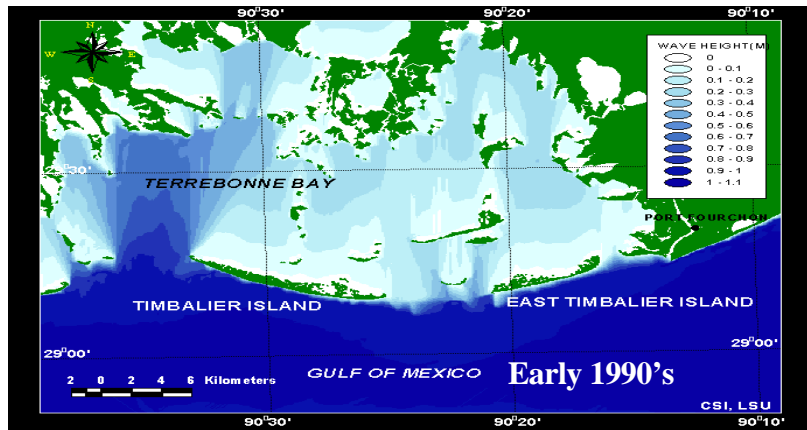


Figure 6. Numerically derived wave field under fairweather, deep water wave conditions along the Isles Dernieres. Note increase in wave height behind the barriers with time as the barrier system erodes. The simulated restored barriers demonstrate the importance of barriers in reducing wave energy in these bays and, therefore, marsh protection.

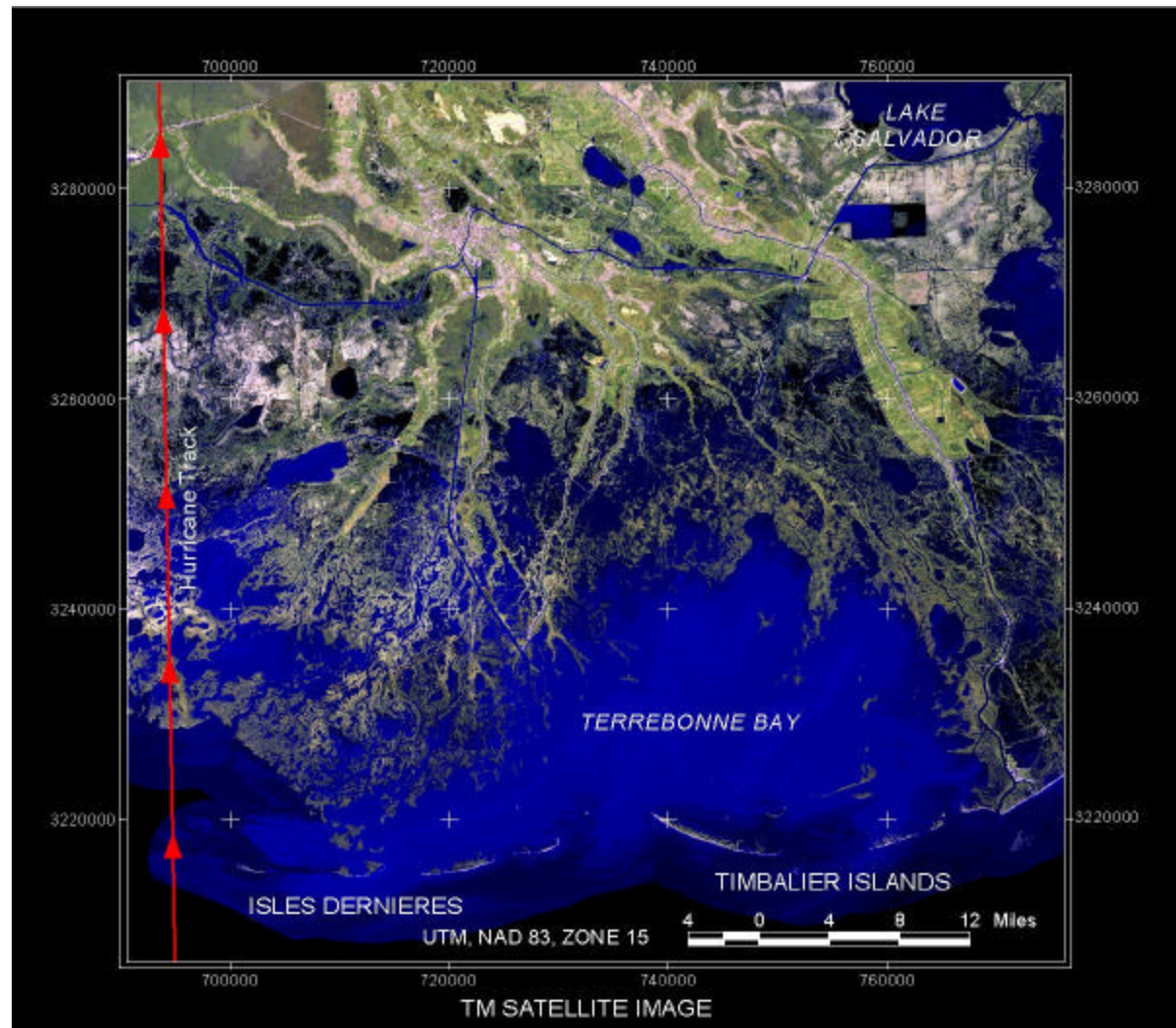


Figure 7. Location of study site in south-central Louisiana including Isles Dernieres and Timbalier islands, north to Lake Pelto. Note, this section of the coast is eroding at the highest rates in Louisiana and the nation. The red sequence of arrows shows the path of the hurricane modeled in this study.

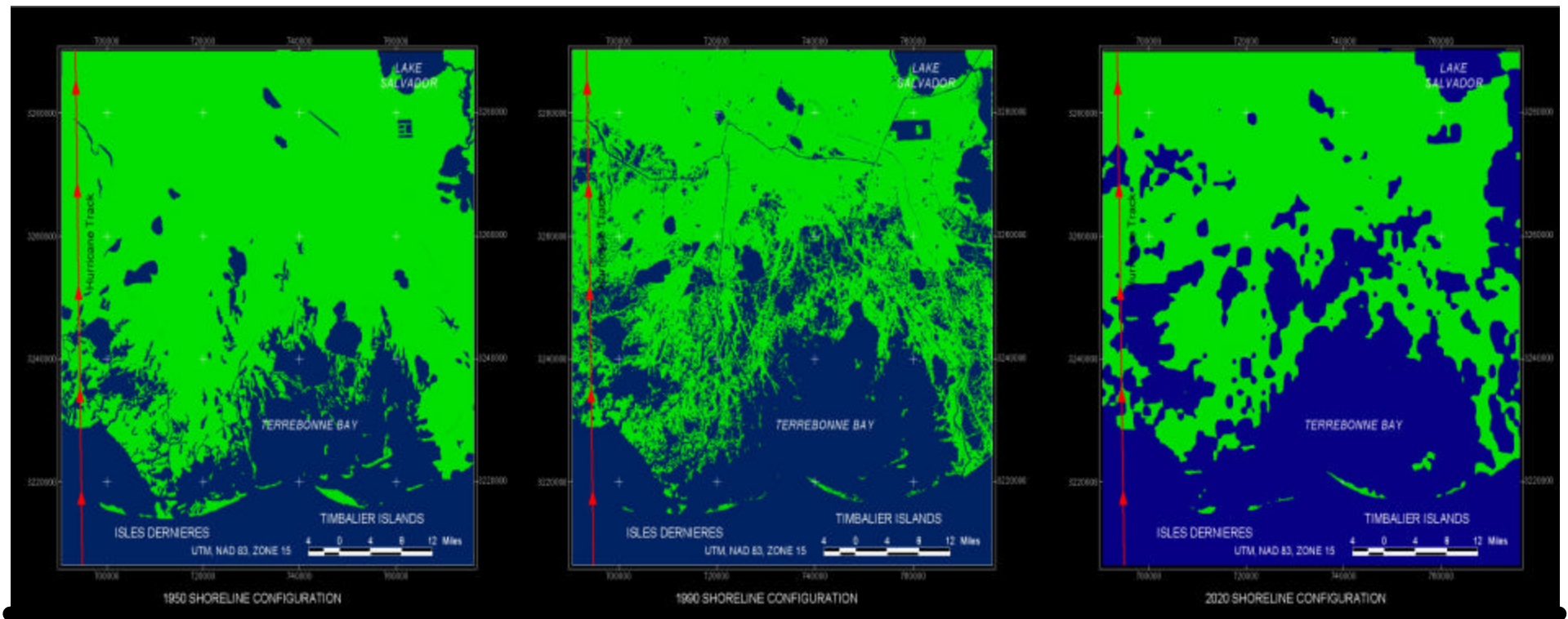


Figure 8. Left: Coastal configuration in 1950 where the study site had ~1.09 million acres of land. Middle: Study site in the early 1990's where the study site had been reduced to ~0.85 million acres of land, a 24% reduction. Right: Forecast loss of land in the study site by the year 2020.

## **METHODS AND NUMERICAL MODEL APPLICATION**

### **Introduction**

Data pertaining to the selection and use of an historic hurricane for application to this project was accomplished using the National Oceanic and Atmospheric Administration's (NOAA) HURDAT data set. This is a comprehensive, online archival data set that is accessible to the public. The numerical modeling component of the project was accomplished using ADCIRC (Scheffner et al., 1994) and SWAN (Booij et al., 1999). ADCIRC is a numerical model capable of computing the time dependent, free surface circulation and transport in two and three dimensions utilizing the finite element method in space. In this project, we use the model to forecast hurricane storm surge and subsequent flooding. SWAN is a sophisticated 3<sup>rd</sup>-generation spectral wave model, designed for the nearshore zone. It is relatively quick to set up and user-friendly in operation. As input, it requires the boundary wave spectrum (minimum requirements are the wave height, period and direction), wind speed and direction and water level. ArcGIS 8.1, and ArcView 3.3 were the primary GIS (Geographical Information System) software package used in this project. Several customized programs were developed to convert the data format and retrieve the data from the model to GIS software. Combined, TIN (Triangulated Irregular Network) and GRID based GIS was the primary approach adopted for this project. A TIN model is a simple way to build a surface from a set of irregularly spaced points. The sample points are connected by lines to form triangles, within each triangle the surface is usually represented by a plane. The GRID model is used to represent the surface by dividing a value (e.g., wave height) into equal-sized cells. The value represents only one specific characteristic. Therefore, each of the parameters is represented by individual GRID models. This approach is discussed in more detail below.

### **Selection of an Historic Hurricane**

Selection of a representative hurricane to model was an important component of this work and received considerable attention. A significant amount of unpublished work in the form of storm surge modeling had already been conducted by the U.S. Army Corps of Engineers (Drs. Norman Scheffner, Coastal and Hydraulics Laboratory, Waterways Experiment Station and Lee Butler, Veri Tech, personal communication). Those data showed conclusively that during simulated Category 4 and 5 hurricanes making landfall in south-central Louisiana, the entire barrier and marsh system was submerged to the point where it became ineffective in even partially mitigating the inshore surge and wave field. Therefore, utilization of such a powerful hurricane would not help meet the objectives of the current project. Also, given the fact that no known Category 4 or 5 hurricanes at landfall have come ashore along the study site and that a historical precedent for a hurricane of this magnitude had not been established, a Category 3 hurricane (at landfall) was selected as the "design storm" for the present effort. Since 1950 four storms with Category 3 strength have made landfall at/near the study site: Hilda (1964), Betsy (1965), Carmen (1974) and Andrew (1992). (For a detailed evaluation of historic hurricanes impacting the Louisiana coast the reader is referred to Stone et al., 1997 and Muller and Stone, 2001).

In flood protection design work, the U.S. Army Corps of Engineers frequently uses a Category 3 hurricane documented as having made landfall slightly west of Grand Isle in 1915 (Dr. Norm Scheffner, personal communication). The track of the system is shown in Figure 9 and the storm is referred to as number 214 on the National Oceanic and Atmospheric Administration's HURDAT data set. The hurricane began moving north-northwest on September 22<sup>nd</sup>, 1915, from the eastern Caribbean Sea, traversed the Gulf as a category 4 storm and made landfall just southwest of Grand Isle, Louisiana, on October 30, 1915. The maximum wind speed was 115 miles per hour with the lowest pressure of 931 mb. The storm was responsible for near 300 deaths in Louisiana.

To fully establish the effects of barrier and wetland loss on storm surge and wave conditions over time, the 1915 hurricane track was perturbed westward 54.4 miles (0.9 degrees) southwest of its original point of landfall (Figure 9). With this trajectory and the meteorological characteristics of the original 1915 hurricane, the wind, surge and wave fields would become maximized over the study site. Thus, “tweaking” of the trajectory when coupled to actual meteorological characteristics of an historic event was deemed appropriate to meet the objectives of the present study; utilization of any other historical event in the category 3 range at landfall would not have permitted meeting the objectives of this project.

## Tropical Storm Wind Field Model

The hurricane wind field model used in conjunction with the ADCIRC model is the Hurricane Planetary Boundary Layer (PBL) model developed by Cardone et al. (1992). This model simulates hurricane-generated wind and atmospheric pressure fields by solving the equations of horizontal motion which have been vertically averaged through the depth of the planetary boundary layer. Additionally, a moving coordinate system is defined such that its origin always coincides with the moving low-pressure center of the eye of the storm  $p_c$ . Therefore, the standard equations of motion are transformed into the following relationships in Cartesian coordinates:

$$\frac{\partial u}{\partial t} + u \frac{\partial u}{\partial x} + v \frac{\partial u}{\partial y} - f v = \frac{1}{\rho} \frac{\partial p_c}{\partial x} + \frac{\partial}{\partial x} K_H \left( \frac{\partial u}{\partial x} + \frac{\partial v}{\partial y} \right) + \frac{C_D}{h} |V| u \quad (1)$$

$$\frac{\partial v}{\partial t} + u \frac{\partial v}{\partial x} + v \frac{\partial v}{\partial y} + f u = \frac{1}{\rho} \frac{\partial p_c}{\partial y} + \frac{\partial}{\partial y} K_H \left( \frac{\partial u}{\partial x} + \frac{\partial v}{\partial y} \right) + \frac{C_D}{h} |V| v \quad (2)$$

where (u,v) are the wind speeds in (x,y) directions,  $\rho$  is the mean air density,  $p_c$  is the pressure field representing the tropical cyclone,  $K_H$  is the horizontal eddy viscosity coefficient,  $C_D$  is the drag coefficient,  $h$  is the depth of the planetary boundary layer, and  $V$  is the magnitude of the wind velocity. The model includes parameterizations of the momentum, heat, and moisture fluxes together with surface drag and roughness formulations. An exponential pressure law is used to generate a circularly symmetric pressure field situated at the low-pressure center of the storm:

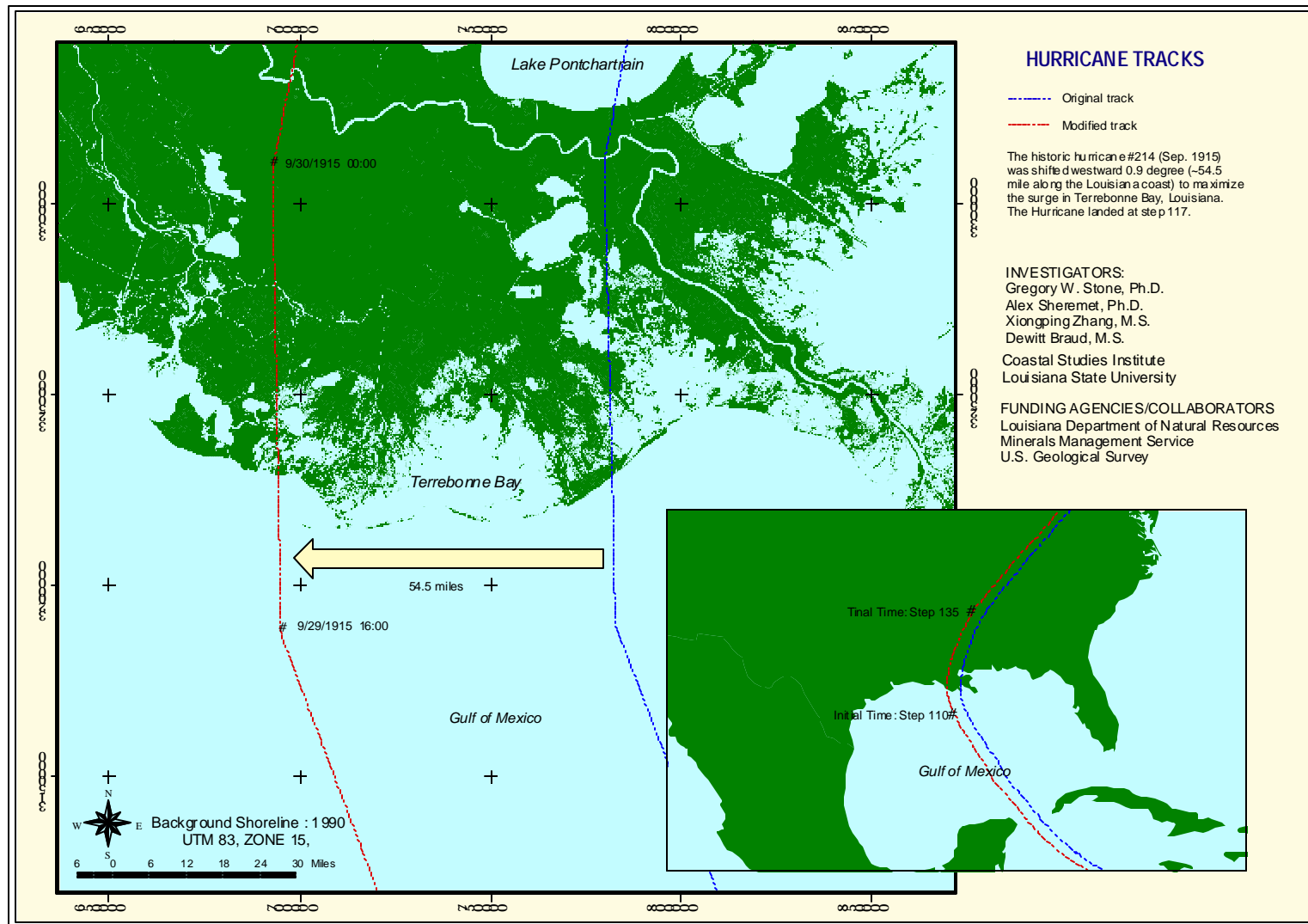


Figure 9. Trajectory of the 1915 storm used in this study after the track is perturbed 0.9 degrees west in order to maximize the wind, surge and wave field at the study site.

$$p_c(r) = p_0 + \Delta p e^{-(R/r)} \quad (3)$$

where  $p_0$  is the pressure at the center or eye of the storm,  $\Delta p = p - p_0$  is the pressure anomaly with  $p$  taken as an average background or far field pressure,  $R$  is the scale radius, often assumed equivalent to the radius to maximum wind, and  $r$  is the radial distance outward from the eye of the storm.

$$\frac{t_x}{r_0} = C_D \frac{r_{air}}{r_0} |V| u \quad (4)$$

and

$$\frac{t_y}{r_0} = C_D \frac{r_{air}}{r_0} |V| v \quad (4)$$

where  $\tau_x, \tau_y$  are the wind stresses in the  $x$  and  $y$  directions, respectively,  $\rho_{air}/\rho_0 = 0.001293$  is the ratio of the air density to the average density of seawater, and  $C_D$  is the frictional drag coefficient.

The PBL model requires a series of input "snapshots" consisting of a set of meteorological parameters defining the storm at various stages of development or at particular times during its life. These parameters include: latitude and longitude of the eye of the storm; track direction and forward speed measured at the eye; radius to maximum winds; central and peripheral atmospheric pressures; and an estimate of the geostrophic wind speed and direction. The radius to maximum winds is approximated using a nomograph that incorporates the maximum wind speed and atmospheric pressure anomaly (Jelesnianski and Taylor; 1973). Peripheral atmospheric pressures were assumed equal to the standard atmospheric pressure of 1013 millibars (mb) and the geostrophic wind speeds were specified as 6 knots in the same direction as the moving eye of the storm. The PBL model input consists of "histogram" and "snapshot" files which define the hourly location in latitude and longitude of the eye of the storm and the storm intensity parameters specified at defined times.

The PBL model computes a stationary wind and pressure field distribution corresponding to the storm characteristics specified in the snapshot file at locations corresponding to the locations of the eye specified in the histogram file. These wind and pressure files are defined on a nested grid composed of five subgrids. Each subgrid measures 21 by 21 nodes in the  $x$ - and  $y$ -directions with the center of all subgrids defined at the eye of the hurricane. Although the number of nodes composing each subgrid is the same, the spatial resolution is doubled for each successive grid. For this study, the center grid with the finest resolution has a  $\Delta x$  and  $\Delta y$  grid spacing of 5 km (3.1 mi). Incremental distances for the remaining subgrids are 10, 20, 40, and 80 km (6.2, 12.4, 24.9 and 49.7 mi). These fixed grids translate with the propagating storm as defined by the histogram file.

The hurricane translational motion is incorporated into PBL model calculations by adding the forward and rotational velocity vector components. A non-linear blending algorithm is then incorporated to generate a nested grid field of wind and pressure for each hour during the life of the storm event. These hourly wind and pressure fields are then interpolated from the PBL nested grid onto the hydrodynamic model grid and subsequently stored for use by the ADCIRC model. Although the PBL model is idealized and modifications in stress are not made for changing sea state and/or landfall, surge results have been shown to be acceptable (Mark and Scheffner 1997; Scheffner et al., 1994).

Snapshot and histogram files are computed from data contained in the National Oceanic and Atmospheric Administration's (NOAA) National Hurricane Center's DATAbase (HURDAT) of tropical storm events (Jarvinen et al., 1988). This database contains descriptions of all hurricane, tropical storm and severe tropical depressions which have impacted the east coast, Gulf of Mexico, and Caribbean Sea from 1886 to present. The database contains latitude and longitude locations of the eye of the hurricane with the corresponding central pressure and maximum wind speeds at 6-hour intervals.

## **Numerical Model ADCIRC**

Storm surge associated with the hurricane was simulated using ADCIRC, a highly developed computer program for solving the Boussinesq approximations of the equations of motion for a moving hydrostatic fluid on a rotating earth (Luettich et al., 1992). The model uses a finite element discretization method for the spatial domain and finite differences in the time domain. ADCIRC can be run either as a two-dimensional depth integrated model or as a three-dimensional model. In either case, elevation is obtained from the solution of the depth-integrated continuity equation in Generalized Wave-Continuity Equation (GWCE) form. Velocity is obtained from the solution of either the 2DDI or 3D momentum equations. All nonlinear terms have been retained in these equations. ADCIRC has been optimized by unrolling loops for enhanced performance on multiple computer architectures. ADCIRC includes MPI library calls to allow it to operate at high efficiency (typically better than 90 per cent) on parallel computer architectures. Simulations of flow and elevation were forced by boundary conditions including a zero normal flow, no slip conditions for velocity, surface stresses and atmospheric pressure fields generated by the hurricane model.

The unstructured grid used for storm surge simulations based on ADCIRC is shown in Figure (10). The grid covers the entire basin of the Gulf of Mexico, at a resolution that increases across the shelf and inshore. This increase in resolution facilitates detailed simulations of storm surge flooding. A larger scale image of the spatially distributed data point locations is shown for coastal Louisiana in Figure 11. The actual computational grid developed for wave modeling purposes is shown in Figure 12 and is composed of two sub-grids: Coarse (4 km, 2.5 mi) Gulf of Mexico basin scale; and Fine (300 m, 985 ft) local scale encompassing the study site.

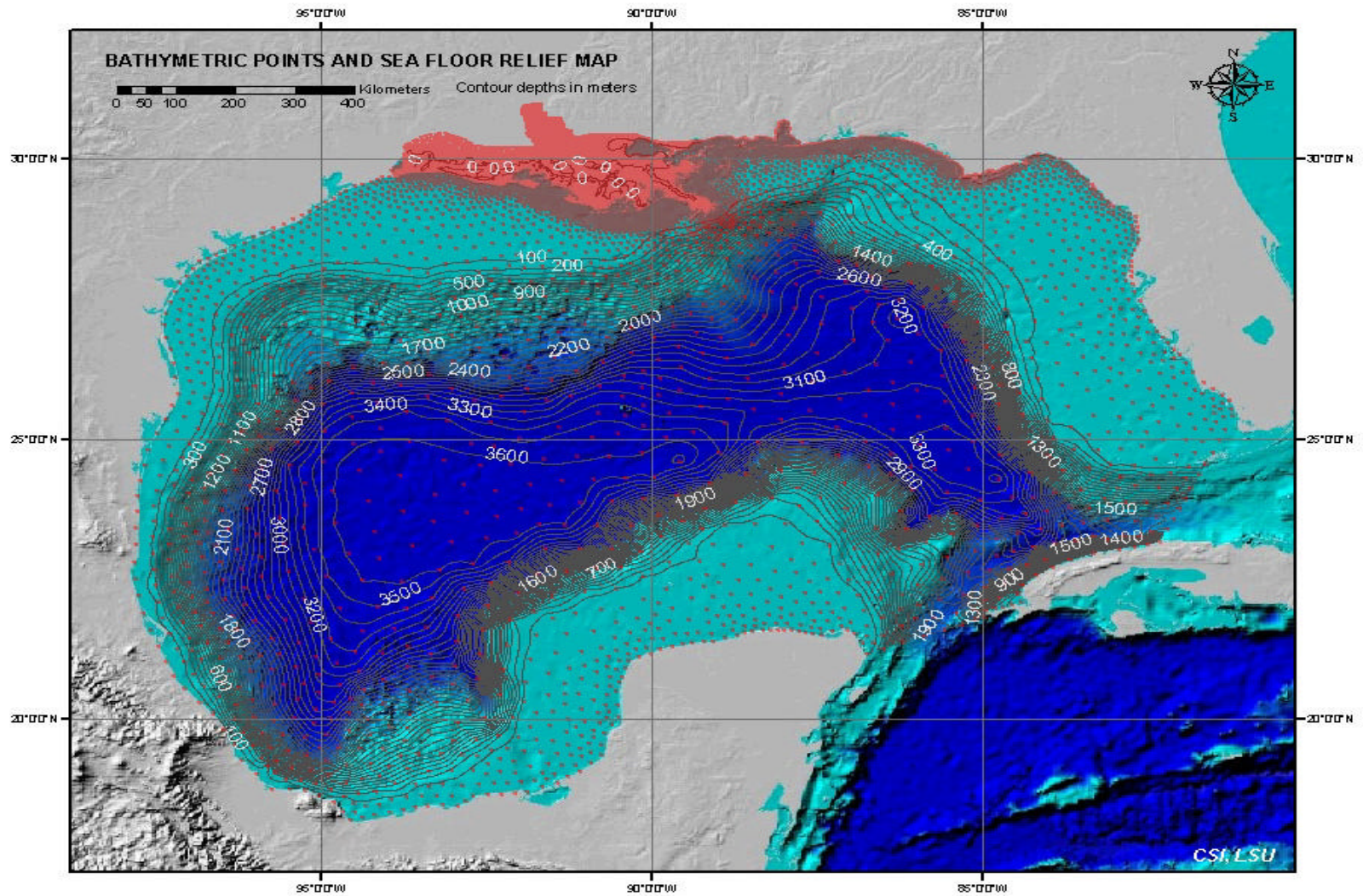


Figure 10. Unstructured grid showing 49156 elements and 25108 nodes where bathymetry and topographic elevation values were obtained for modeling.

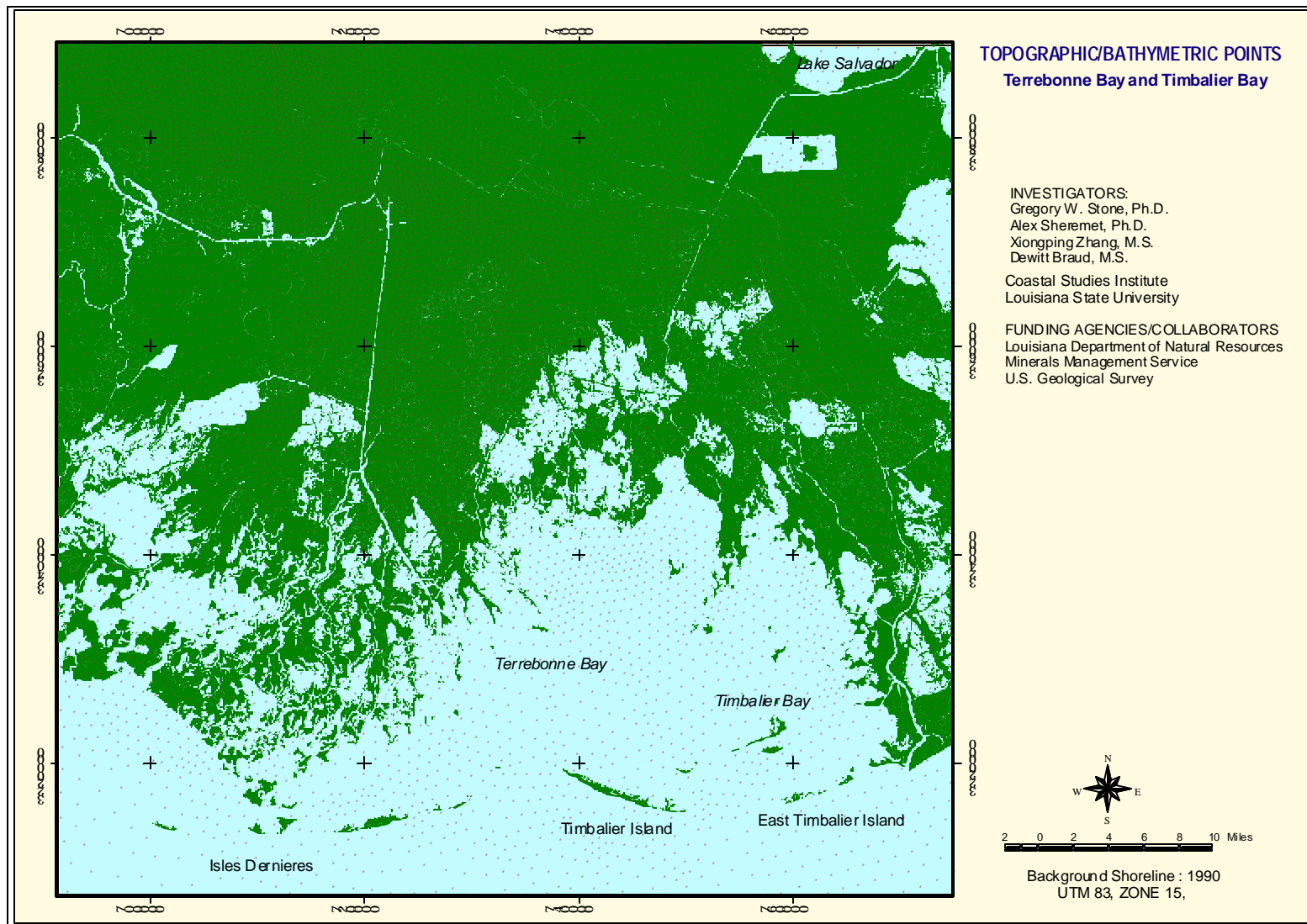


Figure 11. Map of spatially distributed data points for the Louisiana coast where depth and topographic values were obtained for modeling.

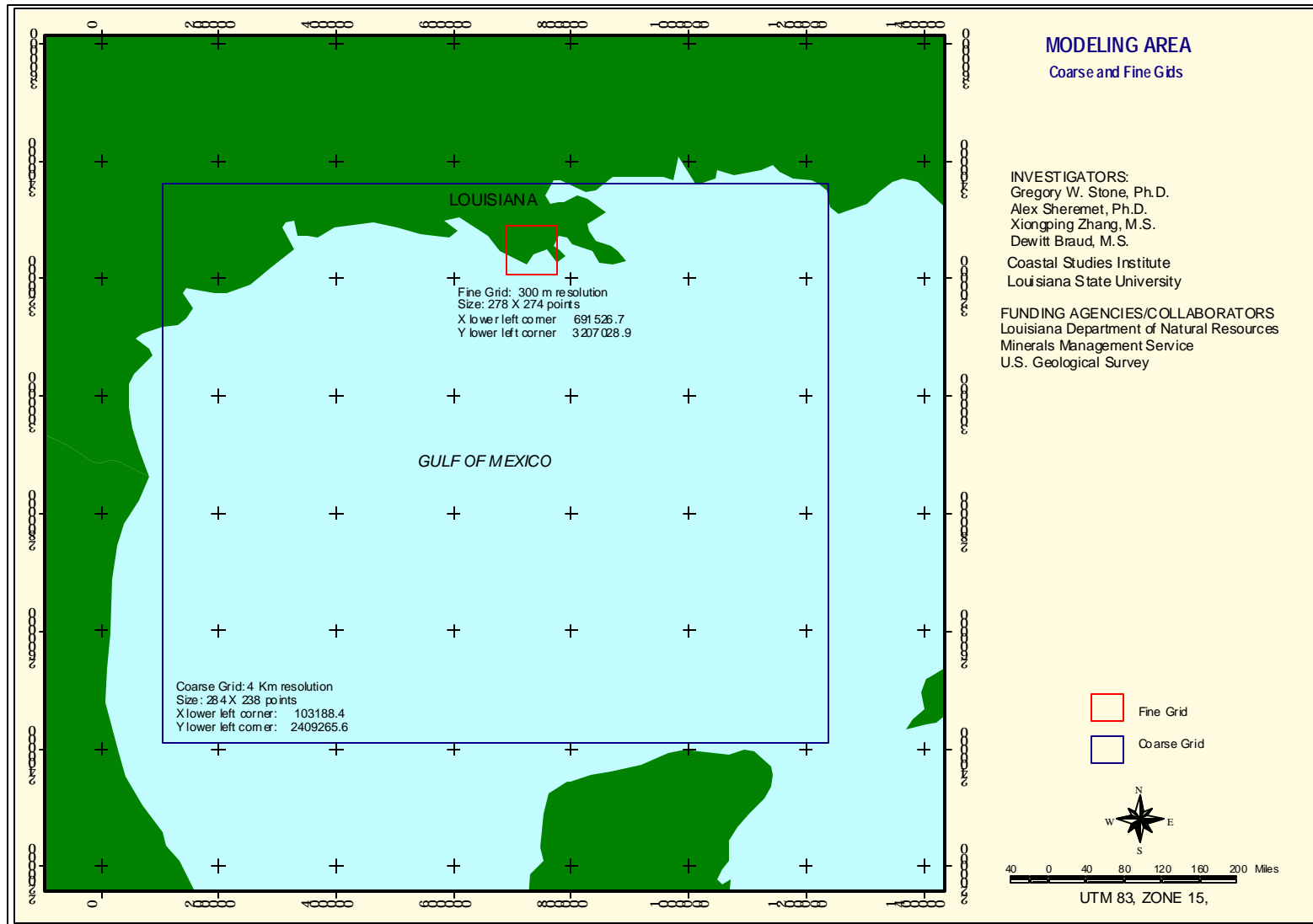


Figure 12. Coarse (4 km, 2.5 mi) Gulf of Mexico basin scale and Fine (300 m, 985 ft) local scale encompassing the study site.

## Numerical Model SWAN

High energy conditions and spatial and temporal scales associated with a strong hurricane such as the 1915 storm, impose severe requirements on numerical simulations of ocean wave propagation, limiting considerably the choice of numerical models. Time domain models are very accurate, however, the need to resolve phase evolution restricts their application to small domains (order of 10 wavelengths). First and second generation spectral models, which assume a known spectral shape, will likely fail over the shelf and in the nearshore, where strong wave energy transfers across the spectrum occur due to nonlinear four- and three-wave interactions which are expected to dominate the energy balance. In this study, wave propagation is simulated numerically using a nonstationary third generation nonlinear model called SWAN (Booij et al. 1999). Nonlinear mechanisms (including triad and quartet interactions) are not parameterized, but are represented explicitly in the governing equations. No a-priori assumption is made about the shape of the wave spectrum and its evolution is driven entirely by physical processes. SWAN accounts for most of the linear wave propagation effects (with the notable exception of diffraction and scattering reflection): shoaling, refraction due to current and depth, frequency shifting due to currents and nonstationary depth, and transmission through and reflection from obstacles. It incorporates nonlinear mechanisms for wave generation by wind, three- and four-wave interactions, whitecapping, bottom friction, depth-induced breaking, and wave-induced setup.

Robust advection schemes (Rogers et al., 1999) give SWAN the flexibility to describe wave propagation at a wide range of spatial scales, from laboratory up to global, on both regular and a curvi-linear grids in a Cartesian or spherical coordinate system. SWAN has the capability of nested runs, using as input data provided either by SWAN or any of the commonly used deep-water models (e.g. WAVEWATCH III, Tolman 1991, or WAM, WAMDIG, 1988). SWAN's flexibility regarding spatial scale is useful in modeling the wave field associated with a hurricane. The simulation of long energetic swells requires a large fetch; in contrast, local wave fields associated with water depth variability induced by the storm surge, are characterized by much smaller scales in both time and space. Consequently, the simulations were carried in two steps, which took advantage of SWAN's nesting capabilities. The large scale evolution of the wave field associated with the hurricane was computed on a coarser grid at a resolution of 4 km (2.5 mi) extending over most of the western half of the Gulf of Mexico (Figure 12). The coarse grid is large enough to contain the storm system in its entirety. For the time sequence studied here, the coarse grid omits regions with a maximum wind speed of less than 5 m/s (16.4 ft). As no information was available regarding wind and wave fields for the hurricane, wave energy was assumed negligible outside the region covered by the storm. As the storm system made landfall, the local bathymetry was modified to include water level changes due to storm surge. The effects of tidal currents generated by the surge on waves were neglected. It was also assumed that the forward speed of the hurricane was slow enough and the energy transferred to waves high enough for the associated wave system to attain quasi-stationary, fully developed state. SWAN was run in stationary mode, with each run spanning an hour in experiment time. With the exception of the more problematic three-wave interaction module, which is not robust enough at the scales of this experiment, all the source terms of the model were activated.

Details of the wave field inside Terrebonne Bay and over the flooded areas south of New Orleans were subsequently computed on a fine nested grid at 300 m (985 ft) resolution (Figure 12), with boundary conditions derived from coarse grid simulations.

## **Input Data Preparation for ADCIRC**

Grid and boundary conditions are required for running ADCIRC. The base grid was supplied by the Coastal and Hydraulics Laboratory (CHL), US Army Corps of Engineers. It contains 49156 elements and 25108 nodes and covers the entire Gulf of Mexico with emphasis on the shelf off Louisiana, inshore and onshore to Lake Salvador. Because ADCIRC can be run on highly flexible, irregularly spaced grids, it takes full advantage of this high resolution grid in coastal Louisiana. Three different bathymetric grids were used in this project: 1950, 1990 and 2020. They were generated by superimposing on the base grid provided by CHL the 1950, early 1990's and 2020 shoreline and bathymetric configuration. The 1950 conditions were obtained from a NOAA navigation chart. The 1990's configuration was obtained from a satellite image of 1990 vintage and the bathymetry from the Barrier Island Feasibility Study (BIFS) in which post Hurricane Andrew data were used to establish the bathymetry (Stone and McBride, 1998). The predicted shoreline and bathymetry for 2020 was also taken from the Feasibility study and the methods used can be obtained from BIFS (1999) and Stone and McBride (1998). For each scenario, the respective data sets were overlaid on the original bathymetric nodes and used to formulate three computational grids for running ADCIRC and SWAN.

## **Input Data Preparation for SWAN**

SWAN requires regular grids with equal spatial intervals. ADCIRC provides an unstructured grid with data output at its nodes. Using GIS, the unstructured nodes were converted from latitude and longitude to UTM. On the UTM projection, the surge, bathymetric and wind vectors are created to TIN and converted to GRID for use by SWAN. Two different resolution grids were prepared; a global grid and a higher resolution fine grid. The output from SWAN obtained using the global grid served as input for the fine grid. For each time step, four layers of information were prepared: water depth, abnormal water depth, U component of wind velocity, and V component of wind velocity. Each layer was obtained for the global and fine grid.

## **Output from ADCIRC**

For this project, ADCIRC generated two ASCII files containing two data sets, abnormal water elevation and wind velocity. The first file contained abnormal water elevation time series output for single time steps totaling 156 steps at all nodes in the domain. These values represent the surge generated by the hurricane. The second file contained U,V components of wind velocity time series at all nodes in the model grid. Each time step represented a one hour interval. The hurricane entered the Gulf of Mexico at step 68, and made landfall along the coast at step 117.

## **Output from SWAN**

SWAN generated wave height, wave direction and wave period. Subsequently, maximum wave height, maximum surge, and maximum wave height plus surge height

were calculated by obtaining the maximum values for each of the 156 time steps. Thus, a grid was developed representing respective maximum values at each grid cell for respective periods in time (i.e., 1950, 1990's and 2020). Grids were compared to determine the change in surge, wave height and surge plus wave height for each of the time periods.

## RESULTS and DISCUSSION

### Surge Elevations and Wave Heights

**1950 Configuration:** Maximum surge elevations (SE), wave heights (WH) and surge plus wave heights (SEWH) are presented for the 1950 scenario in Figures 13, 14 and 15. A faint line indicates the shoreline configuration on the barrier coast and bay/marsh shoreline. Surge levels increase from blue shades to red shades on all figures. Gray indicates where land is not flooded according to the model.

Over the barrier islands SE values range from 10-12 ft and in Terrebonne Bay, increase to 14 ft reaching a maximum of 14.5 ft in the marsh along the north-central part of the study area. The surge envelope is clearly evident along the north flank of Terrebonne Bay along the marsh shoreline. Maximum values are denoted by a red triangle on all figures.

WH values are at a maximum offshore Fourchon where 18.9 ft high waves were numerically derived. Significant decreases in WH occur over the barrier islands where values are 6-7 ft. Where inlets/passes occur, storm waves propagate landward into the adjacent bays and attain values of 8-10 ft in Terrebonne Bay. Barrier islands significantly reduce wave energy in their immediate lee. Wave regeneration does occur particularly across the interior marshes north of the bay shoreline attaining values of ~6 ft. West of this location closer to the storm track, wave dissipation occurs across the marsh surface landward from the barrier coast.

SEWH values show a maximum of 24.9 ft at Fourchon. In Terrebonne Bay and along its northern flank, values are typically 20 ft. Dissipation across the marsh surface farther north is clearly evident where SEWH values show a gradual decrease to ~15 ft. East and west of the area values are typically 10-12 ft and 4-6 ft respectively.

**1990's Configuration:** The barrier islands experience SE values of between 12 and 14 ft (Figure 16) prior to the surge peaking over the marsh shoreline along north Terrebonne Bay. Here surge levels are typically 15 ft with a maximum of 15.3 ft along the north-central portion of the study site. West towards the track of the hurricane, surge levels drop dramatically to a few feet.

Maximum WH values occur offshore of Fourchon attaining a value of 18.9 ft within the study area. The amount of wave energy dissipation and subsequent wave height lowering over the barrier islands is readily apparent in Figure 17 where waves are reduced to 6-7 ft and less. Swell propagation into Terrebonne Bay occurs through Cat Island Pass, between the Isles Dernieres and Timbalier Island chains, and approximate 10-12 ft in the bay. Wave regeneration is again noted north of the bay shoreline where WH approximates 7 ft in places. The importance of the barriers in controlling the wave field in Terrebonne Bay is again apparent.

SEWH values are presented in Figure 18. A maximum value of 24.7 ft. occurred off Fourchon. The combined surge and wave envelope is readily apparent between and

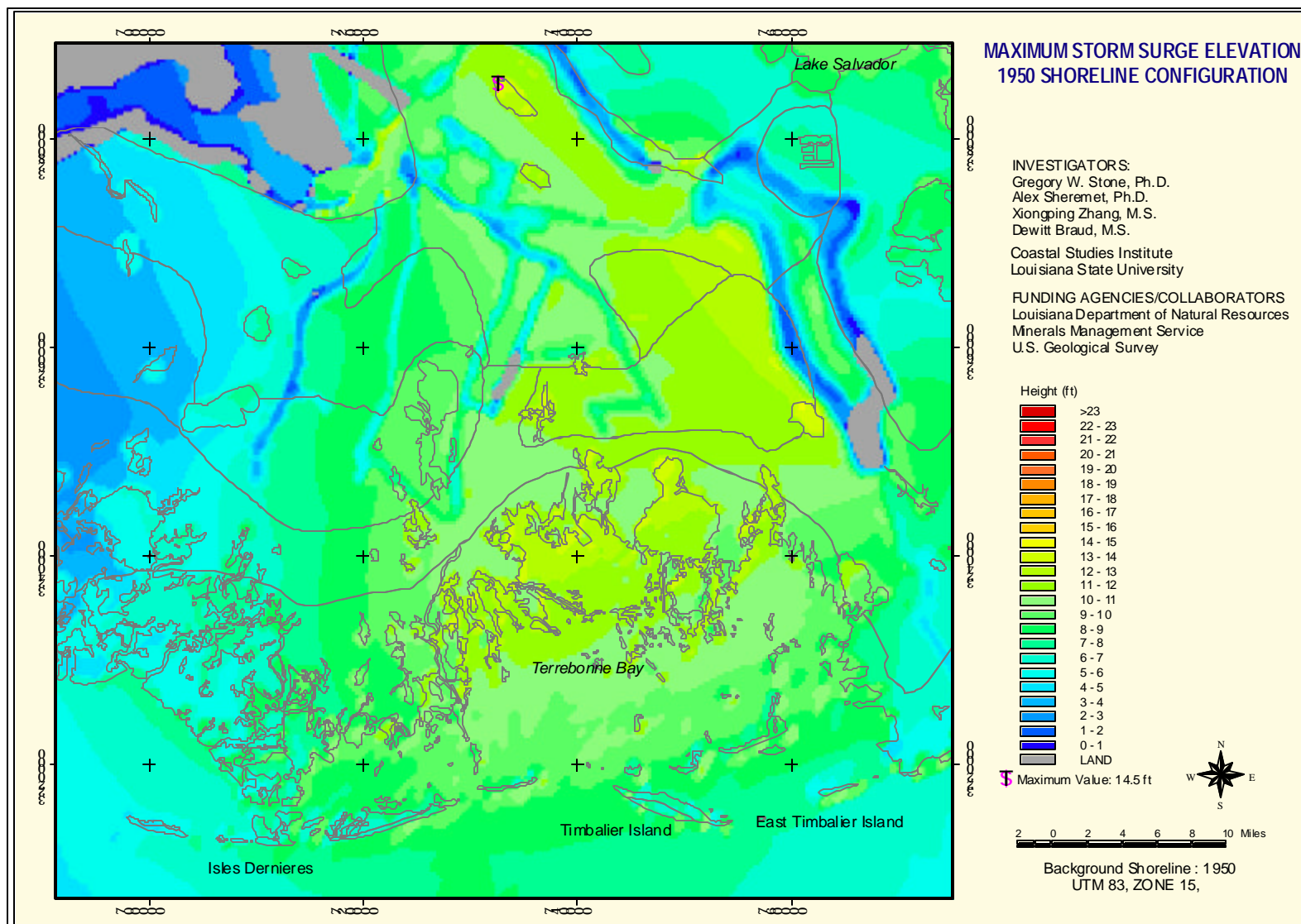


Figure 13. Maximum storm surge elevation along the study site for the 1950 scenario.

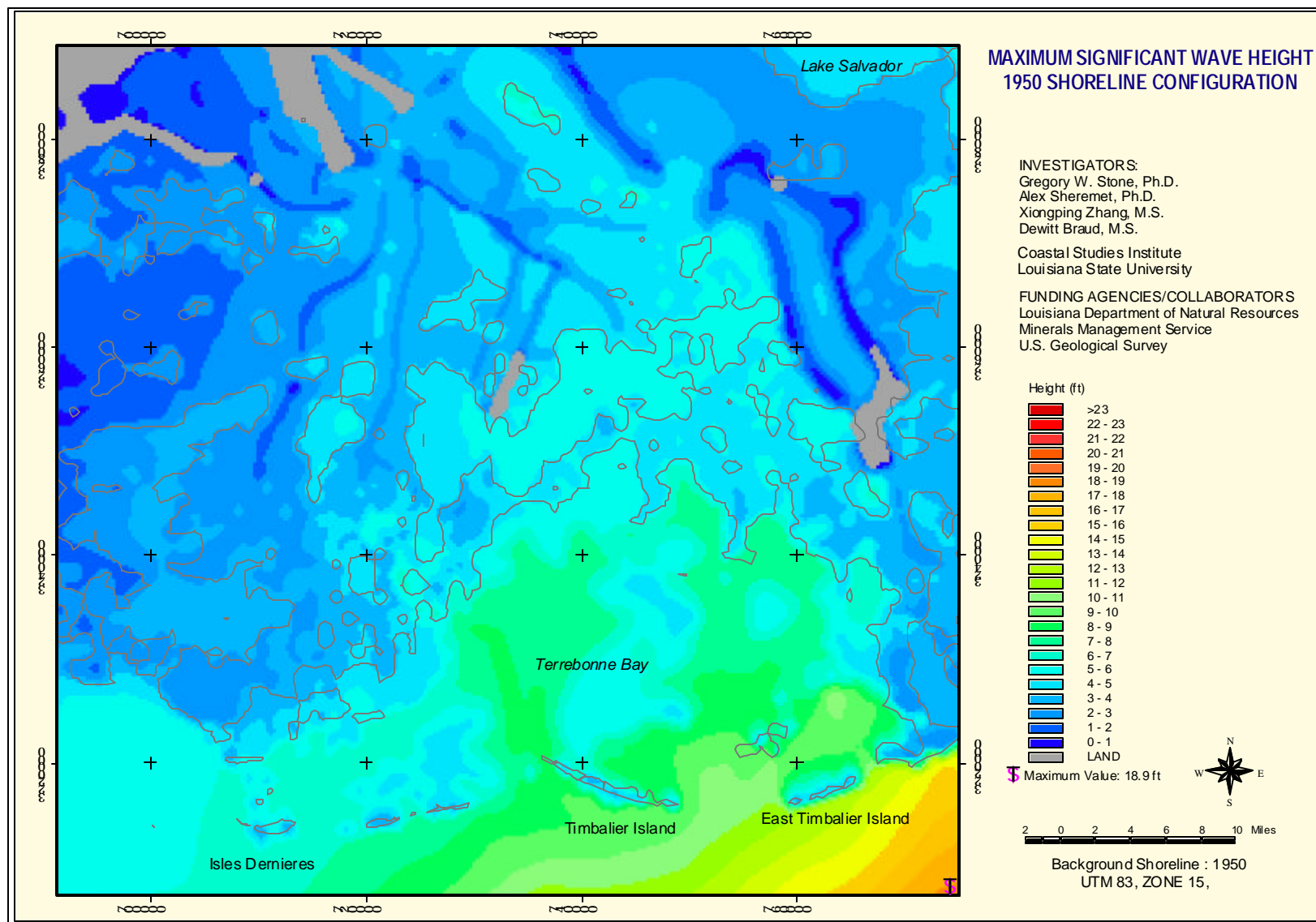


Figure 14. Maximum significant wave height distribution across the study site for the 1950 scenario.

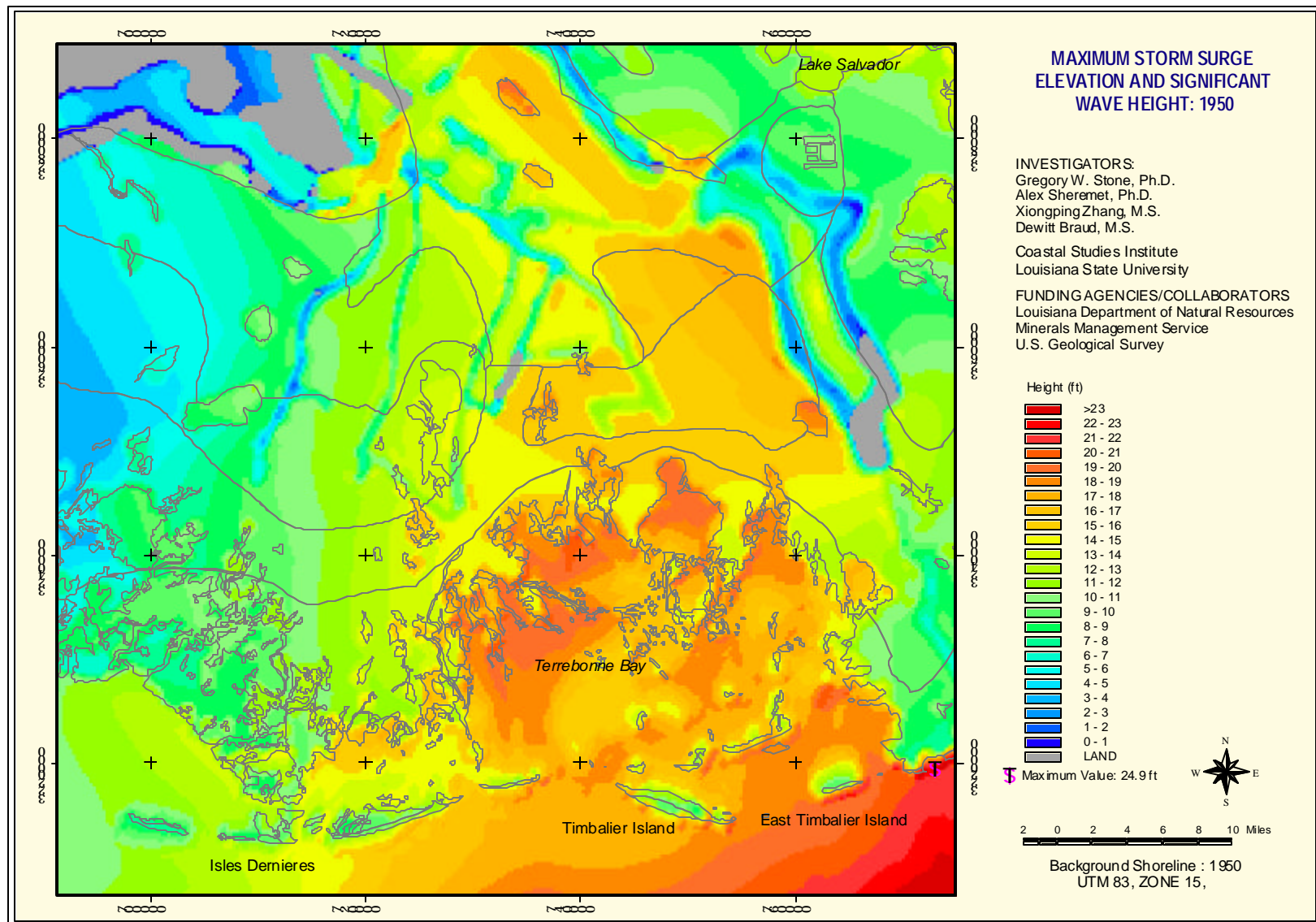


Figure 15. Distribution of maximum surge elevation and significant wave height across the study site for the 1950 sceario.

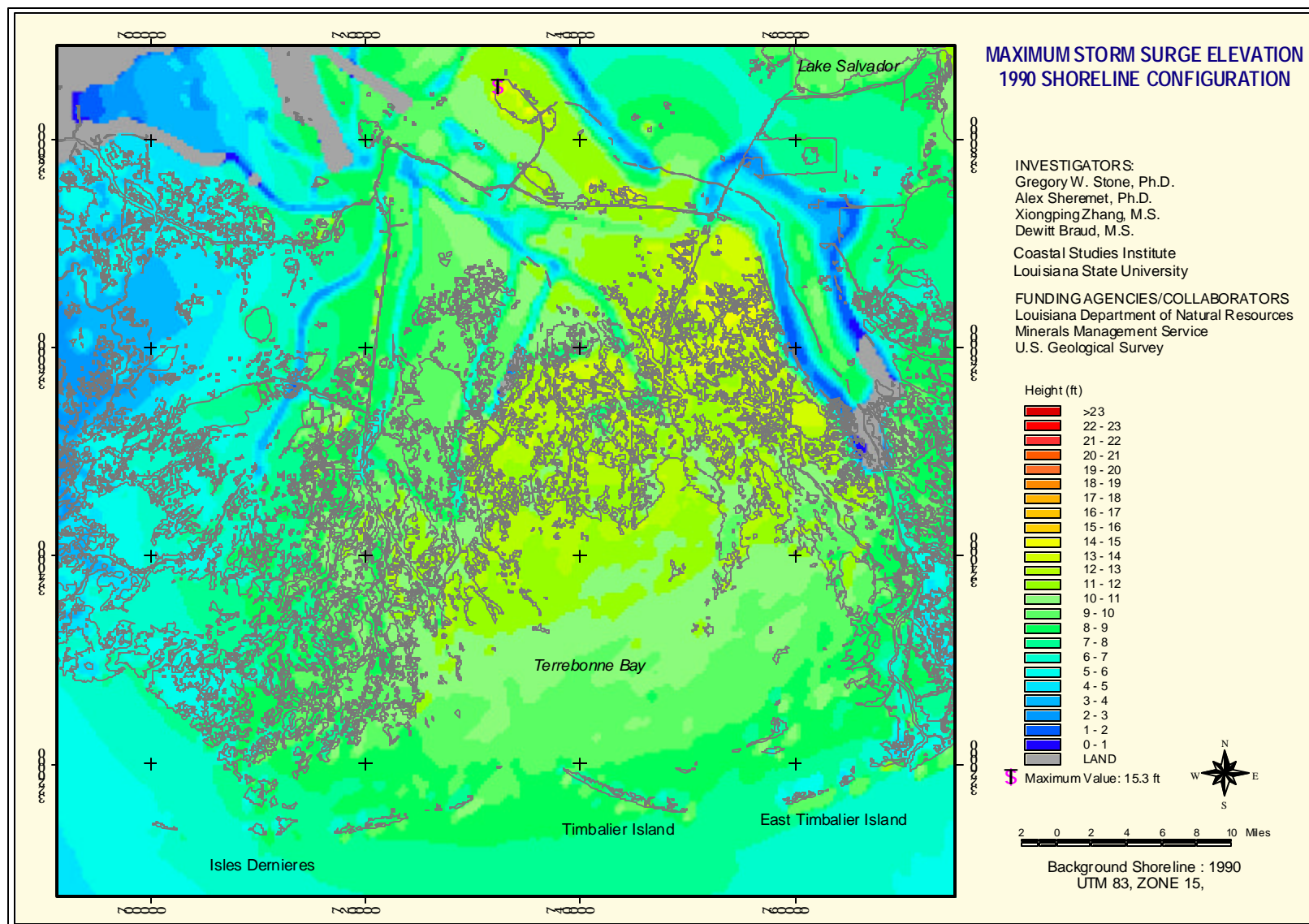


Figure 16. Maximum storm surge elevation across the study site for the 1990's scenario.

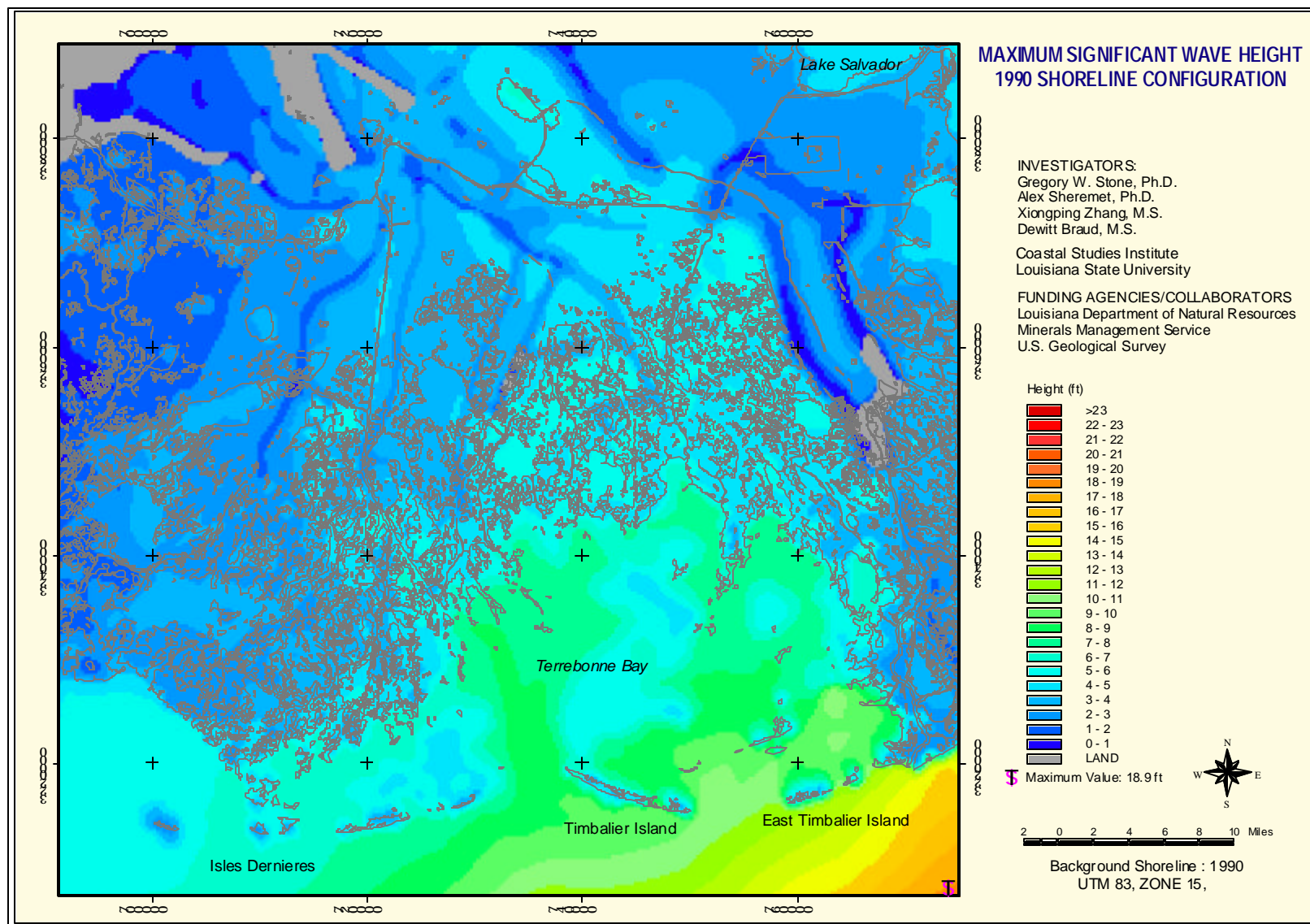


Figure 17. Maximum significant wave height distribution across the study site for the 1990's scenario.

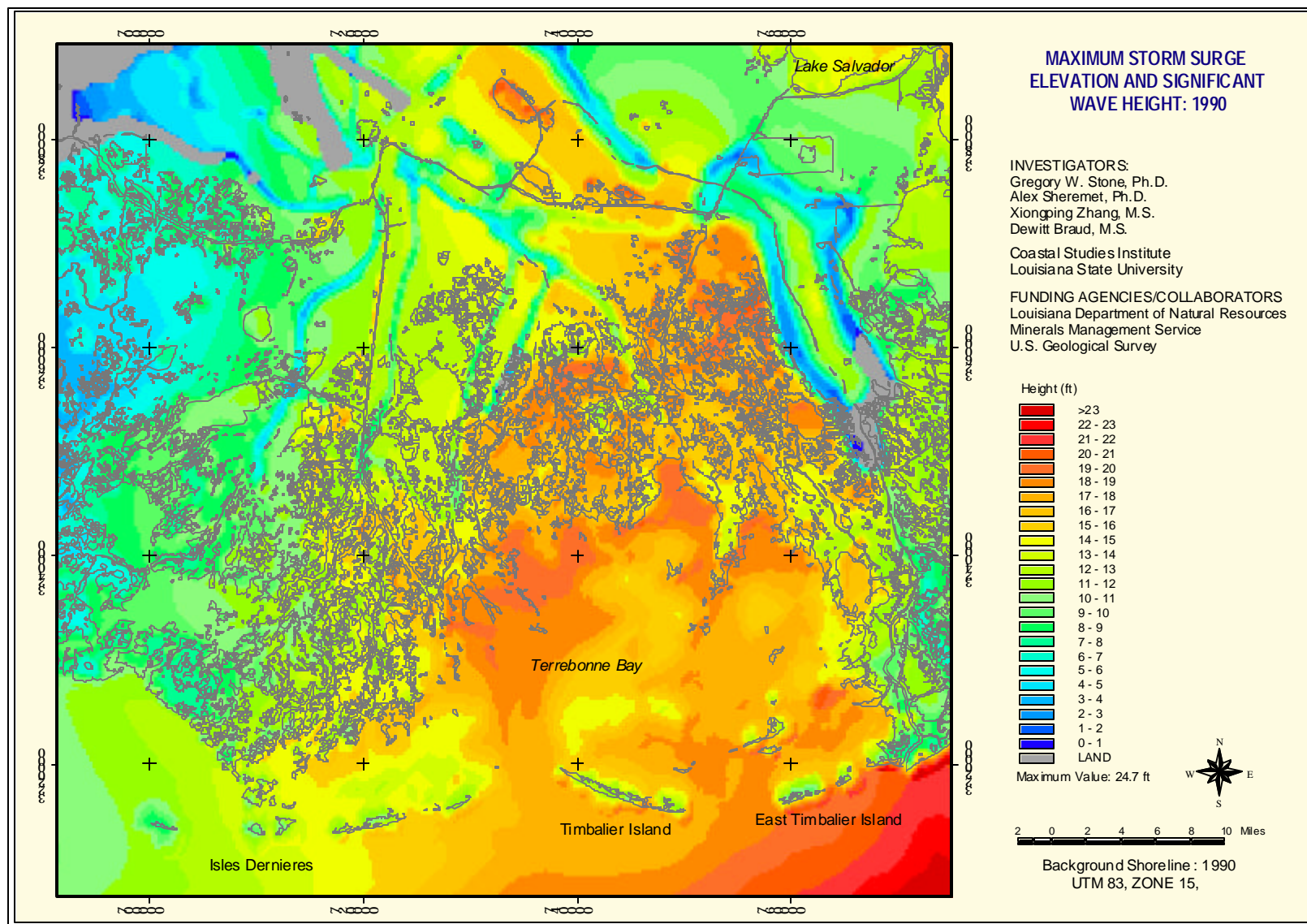


Figure 18. Maximum storm surge elevation and significant wave height distribution across the study site for the 1990's scenario.

landward of Timbalier and East Timbalier Islands north of Cat Island Pass and along the north flank of Terrebonne Bay. Farther north across the marsh, SEWH values exceed 20 ft for the remainder of the northern flank of the study area. This rapidly diminishes to the east and west.

**2020 Configuration:** As shown in Figure 19, surge elevations were approximately 12-14 ft over the barrier islands. North across Terrebonne Bay, surge levels increased to 15 ft and a maximum elevation of 15.3 ft was simulated along the north-central portion of the study site. South of Lake Salvador surge levels were in the 10-12 ft range whereas to the west, closer to the storm track, surge decreased to between 2-4 ft.

Maximum WH values are shown in Figure 20 with the maximum value of 18.9 ft occurring offshore Fourchon. Between the Timbaliers, waves of 10-12 ft in height propagate into the adjacent bay. Propagation of waves between the Isles Dernieres and Timbalier barrier chains at Cat island Pass is very apparent and WH values are in the 10-12 ft range in Terrebonne Bay. The predicted enlargement of the passes along Isles Dernieres results in more storm wave propagation into the adjacent bay and considerable increases in wave energy along the adjacent marshes. This is also evident along the Timbalier chain, although to a slightly less extent. Waves are in the 6-7 ft range along the marsh north of Terrebonne Bay and are rapidly attenuated to the east and west.

SEWH values are presented in Figure 21 and show a maximum value of 24.4 ft off Fourchon. The maximum surge and wave inundation occurs in central and north Terrebonne Bay where 20 ft elevations and greater are common. East and west of this area SEWH decrease rapidly to 10-12 ft and 4-6 ft respectively. The ability of the Isles Dernieres to mitigate the surge and wave field is apparent whereas the Timbaliers exert less of a control.

### **Change in Surge and Wave Height: 1950 - early 1990's**

Changes in maximum storm surge for the 1950-1990's scenarios are presented in Figure 22. The vast majority of the study area experienced storm surge increase over the approximate 40 year time span considered. Much of the area experienced up to a 6 ft increase with the exception of the marsh shoreline in Terrebonne Bay and behind the Isles Dernieres where increases of >12 ft were found; increases in the 10 ft range were more common along Isles Dernieres and Timbalier Islands.

Change in significant wave height is presented in Figure 23. The data reveal a marked increase in wave height throughout the majority of the study site. Larger increases are evident along the marsh bay shoreline and along the barrier islands. Along the marsh shoreline increases of 4 - 5 ft are common whereas on Timbalier Islands 8 ft increases occur. Reduction in wave height is evident at four locations along the barriers and this is directly attributable to island migration to the west along the Timbaliers and to the east along Isles Dernieres. A maximum increase of 10 ft occurs along the eastern portion of East Timbalier.

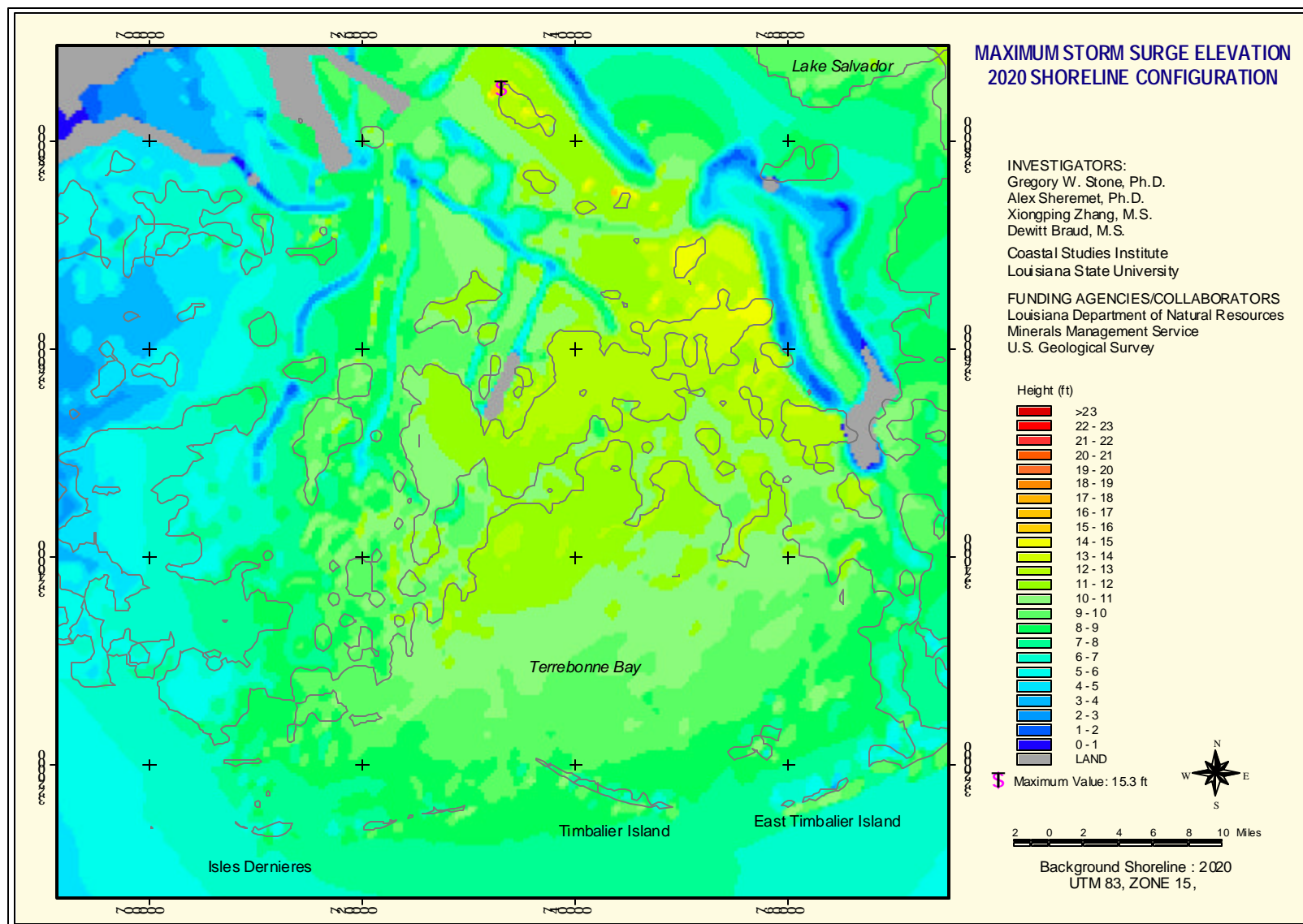


Figure 19. Maximum surge elevation across the study site for the 2020 scenario.

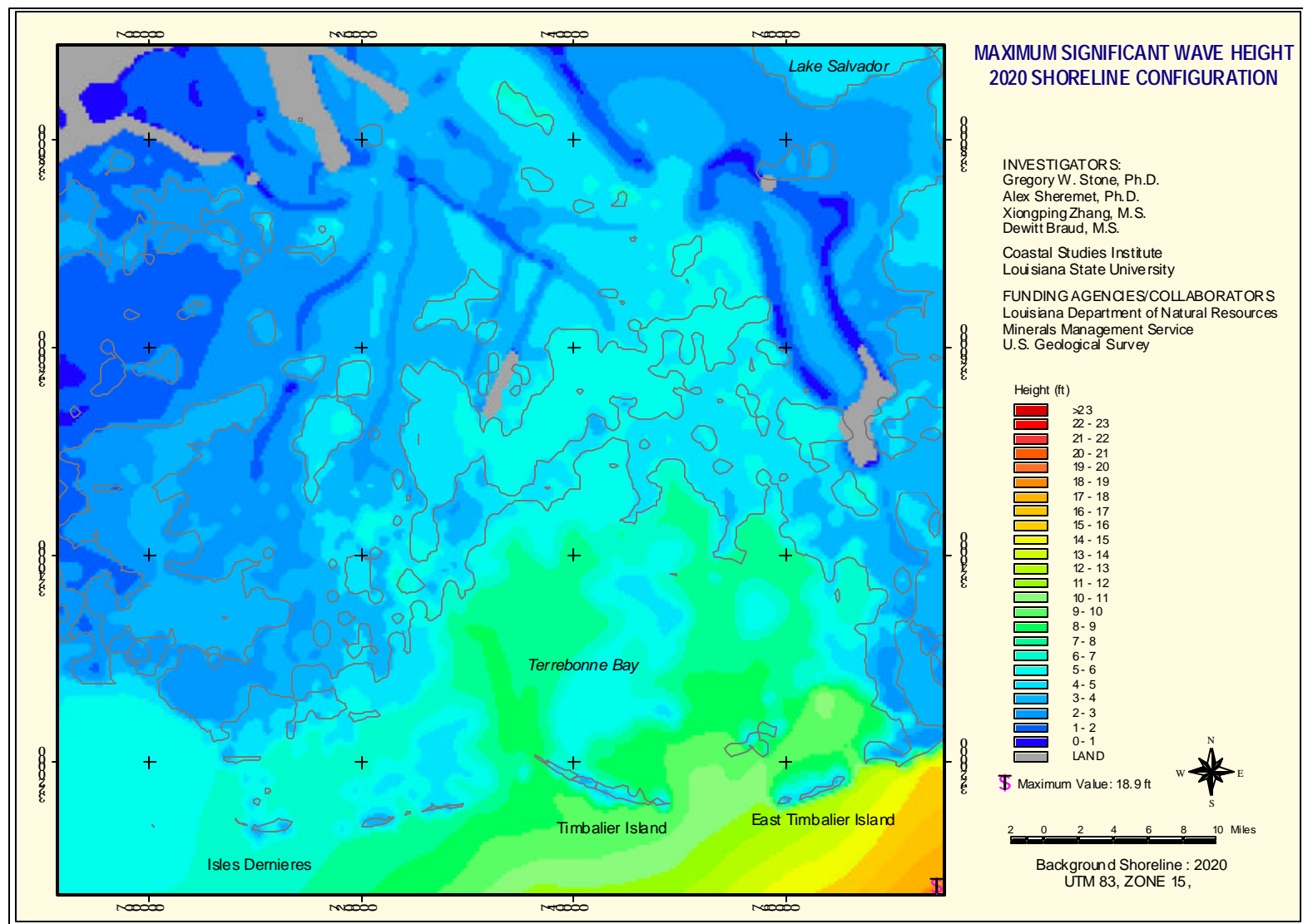


Figure 20. Maximum Significant Wave Height distribution across the study site for the 2020 scenario.

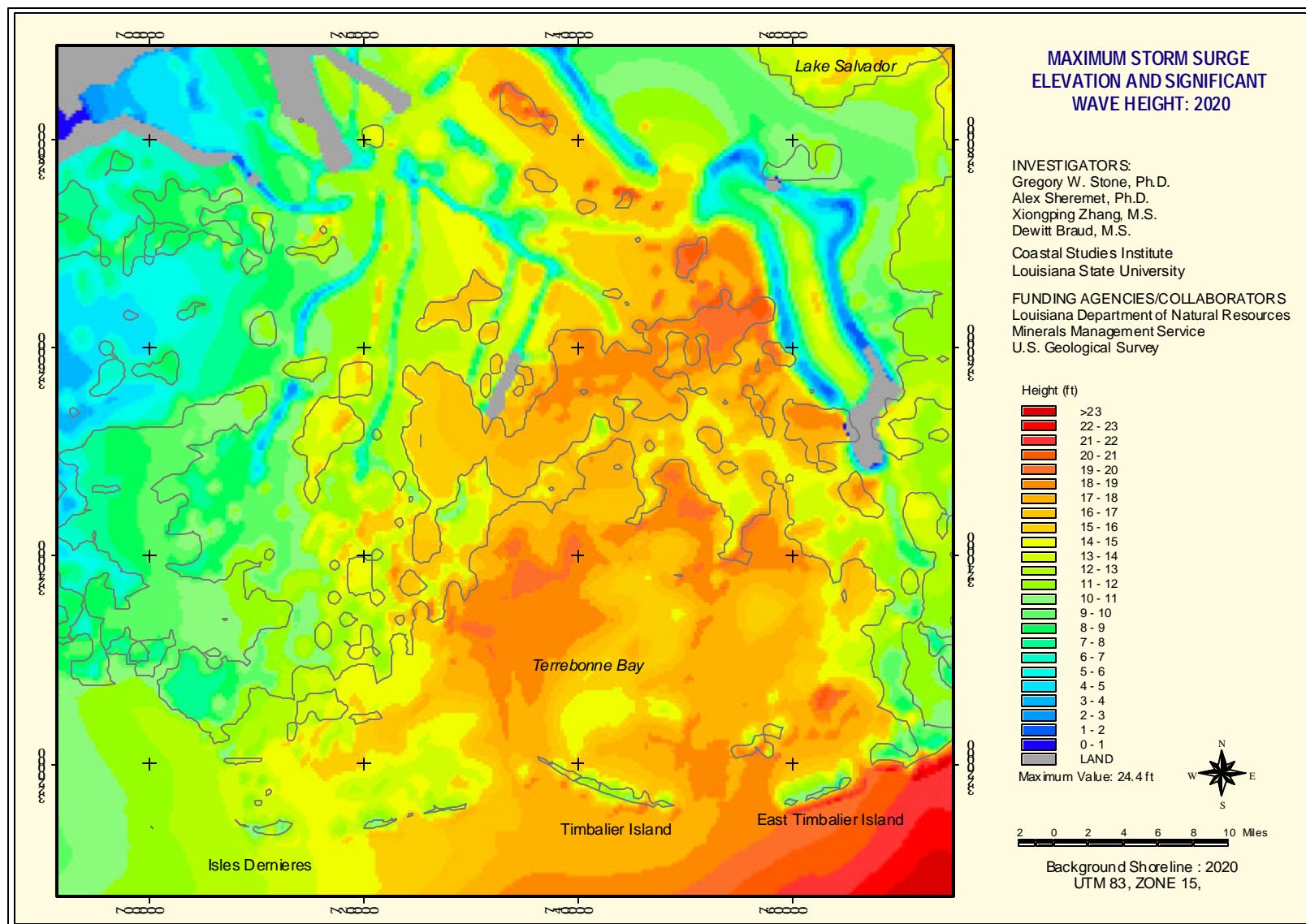


Figure 21. MaximumStorm Surge Elevation and Significant Wave Height for the study area in the 2020 scenario.

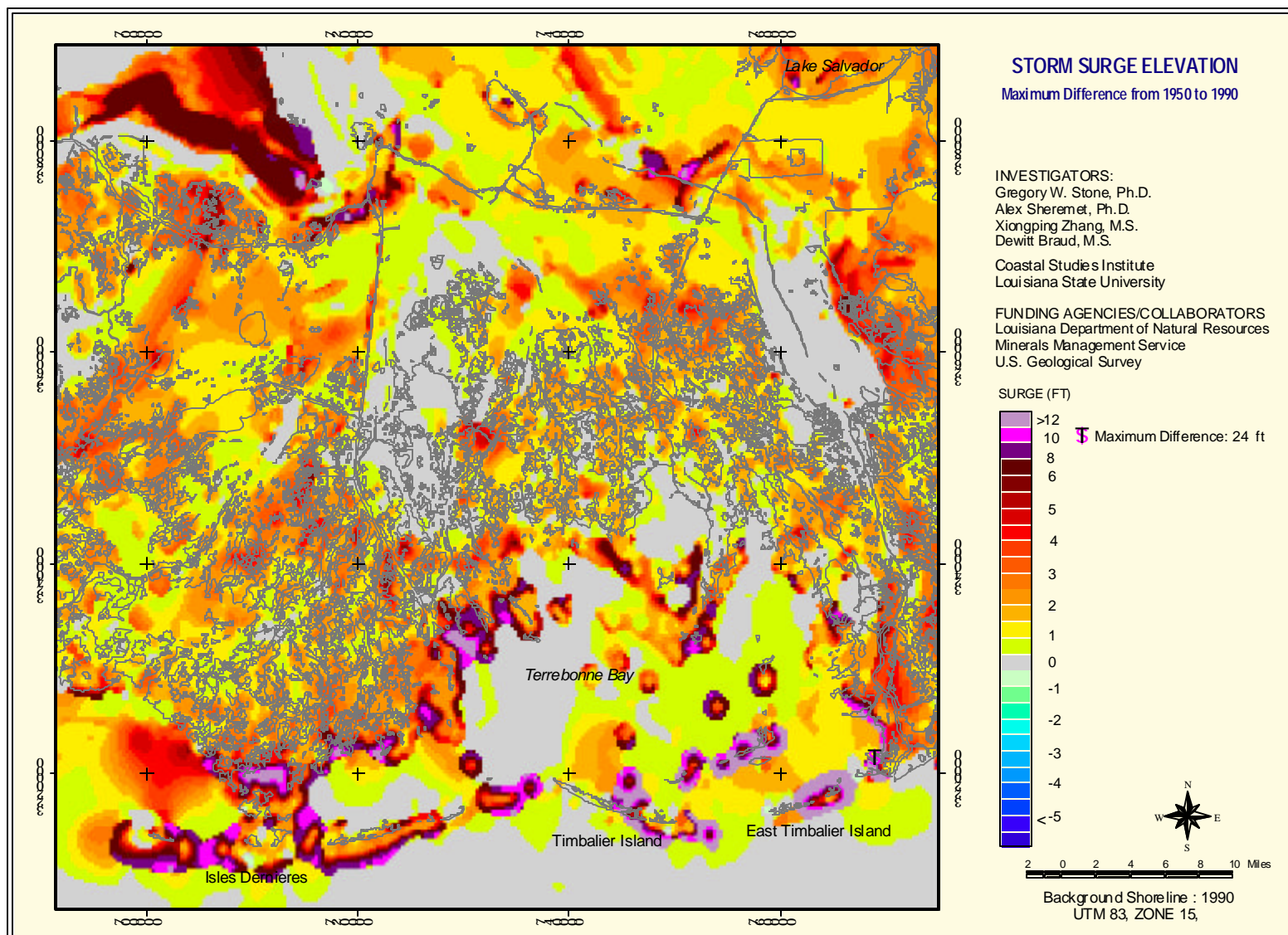


Figure 22. Change in Maximum Surge levels between 1950-1990's across the study area.

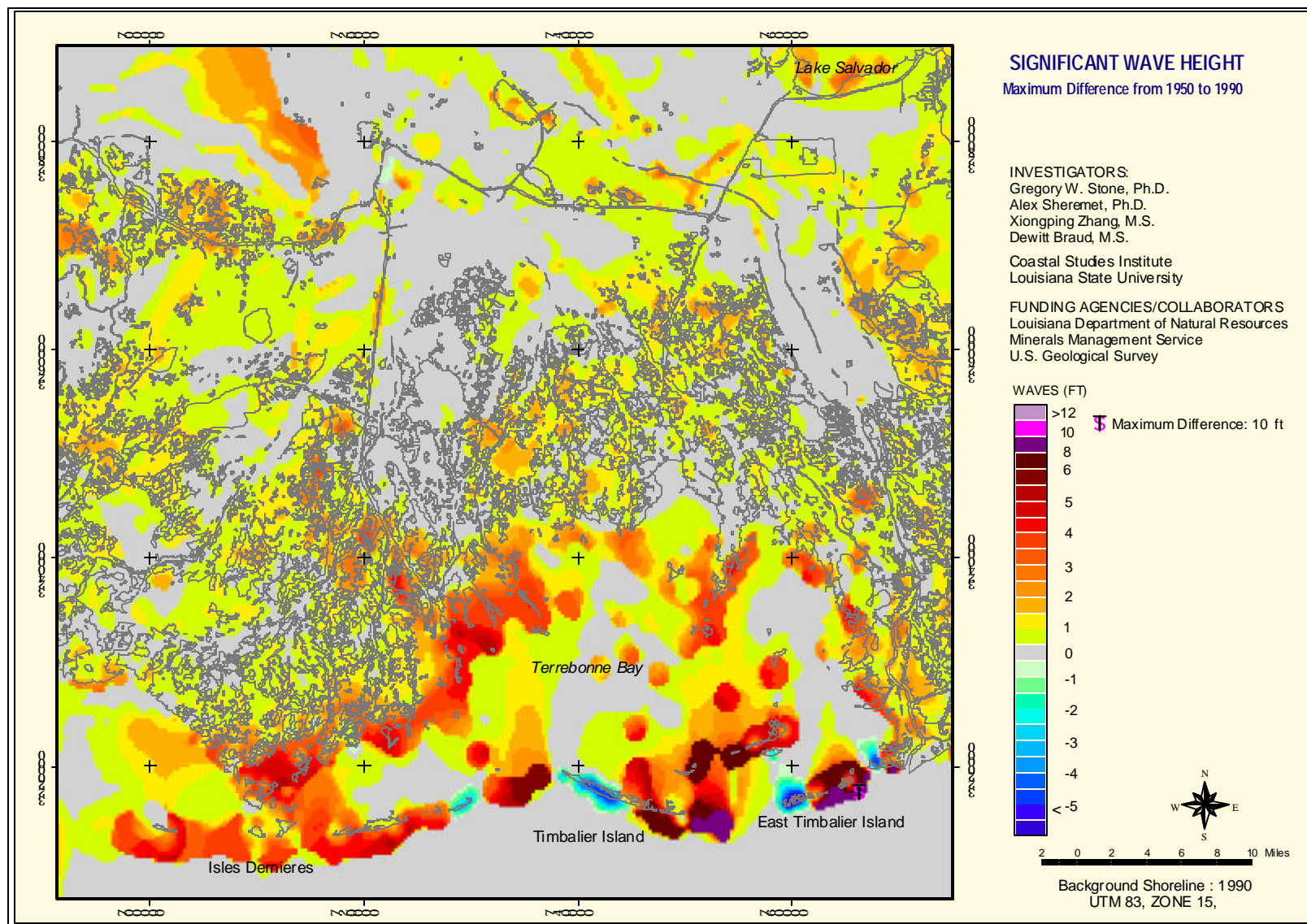


Figure 23. Change in Significant Wave Height between 1950 and 1990's across the study area.